Author Manuscript

Author Manuscript

Author Manuscript

Author Manuscript

HHS Public Access

Author manuscript

Neuron. Author manuscript; available in PMC 2024 June 07.

Published in final edited form as:

Neuron. 2023 June 07; 111(11): 1812–1829.e6. doi:10.1016/j.neuron.2023.03.013.

Identification of an Essential Spinoparabrachial Pathway for Mechanical Itch

Xiangyu Ren[1,3,6], **Shijia Liu**[2,3,6], **Amandine Virlogeux**[1], **Sukjae J Kang**[2], **Jeremy Brusch**[1], **Yuanyuan Liu**[4], **Susan M Dymecki**[5], **Sung Han**[2,*], **Martyn Goulding**[1,7,*], **David Acton**[1,6]

[1]Molecular Neurobiology Laboratory, The Salk Institute for Biological Studies, 10010 North Torrey Pines Rd, La Jolla, CA 92037, USA

[2]Peptide Biology Laboratory, The Salk Institute for Biological Studies, 10010 North Torrey Pines Rd, La Jolla, CA 92037, USA

[3]Biology Graduate Program, Division of Biological Sciences, University of California San Diego, 9500 Gilman Dr, San Diego, CA 92093, USA

[4]NIDCR, National Institute of Health, 35A Convent Drive, Bethesda, MD 20892, USA

[5]Department of Genetics, Harvard Medical School, 77 Avenue Louis Pasteur, Boston, MA 02115, USA

[6]These authors contributed equally

[7]Lead contact

SUMMARY

The sensation of itch is a protective response that is elicited by either mechanical or chemical stimuli. The neural pathways for itch transmission in the skin and spinal cord have been characterized previously, but the ascending pathways that transmit sensory information to the brain to elicit itch perception have not been identified. Here, we show that spinoparabrachial neurons co-expressing *Calcrl* and *Lbx1* are essential for generating scratching responses to mechanical itch stimuli. Moreover, we find that mechanical and chemical itch are transmitted by separate ascending pathways to the parabrachial nucleus, where they engage separate populations of FoxP2^{PBN} neurons to drive scratching behavior. In addition to revealing the architecture of the itch transmission circuitry required for protective scratching in healthy animals, we identify the cellular

*Correspondence: goulding@salk.edu; sunghan@salk.edu.

AUTHOR CONTRIBUTIONS

Behavioral testing and data analysis: X.R., D.A. and S.L. Electrophysiological recordings: D.A. Surgeries and *in vivo* calcium imaging: X.R., S.L., A.V and S.J.K. Histology: D.A., X.R., A.V., and J.B. Y.L. provided retroAAV viruses. S.D. generated the RC::FPSit mice. Experimental design: D.A., X.R., S.L., S.H. M.G. Writing: D.A., X.R., and M.G.

Publisher's Disclaimer: This is a PDF file of an unedited manuscript that has been accepted for publication. As a service to our customers we are providing this early version of the manuscript. The manuscript will undergo copyediting, typesetting, and review of the resulting proof before it is published in its final form. Please note that during the production process errors may be discovered which could affect the content, and all legal disclaimers that apply to the journal pertain.

DECLARATION OF INTERESTS

The authors declare no competing interests.

INCLUSION AND DIVERSTY

We support inclusive, diverse and equitable conduct of research.

Author Manuscript Author Manuscript Author Manuscript Author Manuscript

mechanisms underlying pathological itch by showing the ascending pathways for mechanical and chemical itch function cooperatively with the FoxP2^{PBN} neurons to drive chronic itch and hyperknesis/alloknesis.

eTOC

Ren et al., show Calcrl/Lbx1^{+} projection neurons that relay mechanical- but not chemical-itch from the spinal cord to the parabrachial nucleus are required in vivo for scratching. Labeled line transmission of itch is maintained in the dorsal PBN where separate populations of FoxP2 neurons mediate mechanical versus chemical itch responses.

Keywords

Mechanical Itch; Spinoparabrachial Projection Neurons; Parabrachial Nucleus; Chronic Itch; Alloknesis/Hyperknesis

INTRODUCTION

Itch functions as a protective mechanism that is generated either mechanically by light touch or by pruritogenic chemicals, with recent studies showing that mechanical and chemical stimuli activate molecularly distinct signaling pathways in the periphery and spinal cord[1–4]. Mechanical itch is mediated by spinal neurons that are marked by the expression of the neuropeptide Y (NPY) receptor Y1[3] and Ucn3::Cre[2], whereas chemical itch is dependent on spinal neurons expressing the gastrin releasing peptide receptor (Grpr)[5,6]. Moreover, mechanical and chemical itch are differentially gated by distinct populations of spinal inhibitory neurons[4,7].

Scratching can be elicited by a spinal reflex pathway that persists following cervical transection[8–10], however, expression of this reflex in intact animals requires the activation of supraspinal pathways[11,12]. Moreover, itch is a multidimensional sensation incorporating sensory-discriminative, cognitive, evaluative, affective and motivational components that are subserved by supraspinal centers[13], and chemical-itch stimuli have been shown to activate brain regions associated with affective responses to aversive stimuli, the evaluation of threat, and the planning and initiation of protective motor behaviors[14–18]. Pruritogens also induce conditioned place aversion and anxiety-like behaviors in mice, which can be recapitulated by the activation of itch-responsive neurons in the amygdala[18–20].

The ascending spinal pathways that transmit itch information from the spinal cord to supraspinal centers have not been described in detail. Consequently, it is not known if mechanical and chemical itch are transmitted by a common population of spinofugal neurons or by separate populations, nor is it clear whether these spinal projection neurons share the same cellular targets supraspinally. Whereas the parabrachial nucleus (PBN), and in particular the external lateral nucleus (PBNel), have been shown to mediate protective behavioral responses to chemical itch[11,12], the roles, if any, the PBN and spinoparabrachial (SPB) pathways play in transmitting mechanical-itch signals are unknown. Here we identify an essential population of SPB neurons for mechanical-itch transmission from the spinal

Author Manuscript Author Manuscript Author Manuscript Author Manuscript

cord to the PBN. These neurons are distinct from the SPB neurons that transmit chemical itch, and this segregation of the two itch modalities is maintained within the dorsal PBN, where mechanical and chemical itch are transmitted by two separate subpopulations of PBN neurons that express *FoxP2*. Finally, we show that the supraspinal transmission pathways for both mechanical and chemical itch are overactivated in models of chronic itch, such that they both contribute to hyperknesis and alloknesis under pathological itch conditions.

RESULTS

The PBN is required for behavioral responses to mechanical itch

To better understand the nature of the supraspinal circuitry that mediates mechanical itch-driven scratching in vivo we focused our attention on the postsynaptic dorsal column (PSDC) and SPB pathways that play major roles in integrating and transmitting innocuous and noxious cutaneous sensory modalities, respectively[21–24]. We first assessed whether the dorsal column nuclei (DCN) that receive light-touch information via the PSDC are required for responses to mechanical itch. To do this we used a mouse model in which spontaneous scratching and scratching responses to light punctate touch stimuli are elevated following the ablation of NPY^{Lbx1} spinal interneurons (INs) in *NPY::Cre;Lbx1*^{FlpO}*;Tau*$^{ds\text{-}DTR}$*;Ai65*$^{ds\text{-}tdTom}$ mice[3,4], and the DCN were silenced following bilateral injection of AAV-hSyn-HA-hM4D(Gi)-mCherry and delivery of CNO(Figure 1A). Whereas silencing the DCN in wild type mice impairs hindpaw sensitivity to punctate touch (Figure S1), there was no reduction in touch-evoked and spontaneous scratching when the DCN was silenced following the disinhibition of the mechanical itch pathway (Figures 1B), thereby demonstrating that mechanical itch is independent of the PSDC-DCN pathway.

By contrast, CNO-mediated silencing of the PBN in NPY^{Lbx1} IN-ablated mice resulted in the strong suppression of both touch-evoked and spontaneous scratching (Figures 1C and D). Silencing the PBN also abolished evoked and spontaneous scratching following disinhibition of the mechanical itch pathway in wild type mice by intrathecal (i.t.) injection of the NPY receptor Y1 antagonist BIBP 3226 (Figure 1E). Finally, silencing of the PBN in unsensitized wild type mice resulted in the abolition of touch-evoked scratching (Figure 1F). Together these results demonstrate that the PBN is essential for the expression of protective scratching in response to mechanical-itch stimuli, both in unsensitized wild type mice and in mice sensitized to mechanical itch stimuli.

Mechanical itch is transmitted by SPB neurons expressing *Calcrl*

In characterizing candidate SPB populations that are competent to transmit mechanical-itch information, we identified a group of excitatory dorsal horn neurons that express calcitonin receptor-like receptor(Calcrl). In *Calcrl*^{Cre}*;Cdx2::FlpO;Ai65*$^{ds\text{-}tdTom}$ mice the axon terminals of $Calcrl^{Cdx2}$ neurons, located below C2[25], were almost exclusively found within the lateral PBN. Projections to other supraspinal regions known to receive direct inputs from the spinal cord were absent, aside from sparce axonal labeling within the DCN (n = 3 mice) (Figure 2A). Strikingly, the dense arborization of $Calcrl^{Cdx2}$ spinal projections within the PBN was almost entirely restricted to the dorsal lateral and superior lateral PBN (PBNdl and PBNsl), with few if any terminals within the external lateral PBN (PBNel), which relays noxious

Author Manuscript Author Manuscript Author Manuscript Author Manuscript

signals to the amygdala and PAG[12,26,27]. Further examination of the termination patterns of the spinal *Calcrl*$^{+}$ neuron population using *Calcrl*^{Cre};*Lbx1*^{FlpO};*Ai65*$^{ds\text{-}SypGFP}$ mice, revealed synaptophysin-GFP-labeled synaptic puncta within the lateral PBN but not within the DCN, nor within the periaqueductal grey (PAG) or thalamus, whichreceive collateral innervation by other populations of SPB neurons (Figure 2B)[28,29]. Consistent with this, retrograde tracing from the PBN using cholera toxin subunit B (CTb) revealed that PBN-projecting Calcrl^{Lbx1} neurons represent 18% of SPB neurons (122/680 CTb^{+} SPB neurons from 4 mice) and are concentrated in laminae I-IIo and the lateral spinal nucleus (LSN) with an additional minority located in laminae IIi-V (Figure 2C and D). We also observed some sparse labeling of cells by tdTomato but not CTb in laminae IIi-IV, which are likely to be spinal interneurons.

We then compared the intersectional expression of tdTomato in Calcrl^{Lbx1} neurons with the broader expression of *Calcrl*^{Cre}, exploiting the inclusion of a Cre-dependent LacZ reporter in the *Tau*$^{ds\text{-}DTR}$ allele that is deleted in cells expressing FlpO[25]. In *Calcrl*^{Cre};*Lbx1*^{FlpO};*Tau*$^{ds\text{-}DTR}$; *Ai65*$^{ds\text{-}tdTom}$ mice, tdTomato is expressed in 38.0 ± 3.5% of Cre^{+} (tdTomato^{+}/LacZ^{+}) neurons (n = 4 mice) and LacZ expression was detected in 10.6 ± 1.1% of cholera toxin subunit B (CTb)-labeled SPB neurons (Figure 2E and F). Consistent with this, we detected faithful expression of tdTomato in CTb^{+} SPB neurons labeled with an antibody against Calcrl, and substantial but incomplete expression of tdTomato in Calcrl-immunoreactive SPB neurons (42/70 Calcrl^{+} SPB neurons from 4 mice) (Figure 2G and H). *Lbx1*^{FlpO} therefore captures a subset of Calcrl-expressing SPB neurons, with the remaining fraction likely belonging to an *Lbx1*$^{-}$ lineage of dorsal horn neurons.

Calcrl^{Lbx1} SPB projection neurons transmit mechanical but not chemical itch

In examining whether the spinal Calcrl^{Lbx1} neurons are essential for relaying mechanical-itch information to the PBN, we observed that intersectional DTR-mediated ablation or hM4D-mediated silencing of the spinal Calcrl^{Lbx1} neuron population abolished scratching responses to mechanical itch stimuli (Figures S2A–G). To selectively assess the role of the Calcrl^{Lbx1} neurons that project to the PBN, SPB Calcrl^{Lbx1} axon terminals were silenced by delivering CNO directly into the PBN of *Calcrl*^{Cre};*Lbx1*^{FlpO};*R26*$^{ds\text{-}hM4D}$ mice via bilaterally implanted cannulae (Figure 2I and J). Silencing these axon terminals substantially reduced touch-evoked scratching compared to controls(Figure 2K). Acute sensitization to touch-evoked scratching induced by Y1 inhibition was also reversed by silencing the Calcrl^{Lbx1} axon terminals (Figure 2L). Importantly, silencing Calcrl^{Lbx1} projections to the PBN failed to attenuate either histaminergic itch induced by intradermal (i.d.) 48/80 (Figure 2M) or non-histaminergic itch induced by chloroquine (Figure 2N). Conversely, hM3D-mediated activation of the Calcrl^{Lbx1} neurons resulted in a strong potentiation of both touch-evoked and spontaneous scratching (Figure S3A–B). Furthermore, when the Calcrl^{Lbx1} neurons were activated concurrently with the silencing of the PBN (Figure S3C), these increases in touch-evoked and spontaneous scratching were abolished (Figure S3D–E). Together these data indicate that the Calcrl^{Lbx1} SPB neurons mediate scratching responses that are dependent on normal functioning of the PBN.

Author Manuscript Author Manuscript Author Manuscript Author Manuscript

Interestingly, while impairing the sensitivity of the plantar hindpaw to light punctate touch (Figure S4A), ablating the Calcrl^{Lbx1} neurons did not alter sensitivity to dynamic touch (Figure S4B), or to mechanical pain (Figures S4C–E), thermal pain (Figures S4F–J) or chronic inflammatory pain (Figure S4K). Ablation of the Calcrl^{Lbx1} neurons also had no effect on gross motor (Figure S4L). These results suggest that the Calcrl^{Lbx1} neurons, including those that project to the PBN, are required for the transmission of light-touch information but not pain.

Calcrl^{Lbx1} neurons constitute a novel subdivision of SPB neurons

We then compared the expression of *Calcrl* with that of other known markers of SPB neurons, using RNAScope to analyze the molecular identities of SPB neurons labeled by injection of rAAV2-CAG-eGFP into the PBN. Of particular interest were *Gpr83* and *Tacr1*, which have been reported to label functionally and anatomically distinct SPB subpopulations that constitute the vast majority of SPB neurons[29]. We detected *Tacr1* in 48.7% *eGFP*$^{+}$ SPB neurons and Gpr83 in 42.5% SPB neurons, with 73.2% of SPB neurons expressing either or both markers. *Tacr1* and *Gpr83* were co-expressed in 22.0% SPB neurons, most of which were located in the LSN (Figure S5A–C). In comparing the expression of *Calcrl* with these established SPB markers, we found very little co-expression of *Cacrl* and *Tacr1* (Figure S5D–F) but substantial overlap in the expression of *Calcrl* and *Gpr83*, with *Gpr83* expression in the vast majority (81.0%) of *Calcrl*$^{+}$ SPB neurons (Figure S5G–I), while *Calcrl* was expressed in 48.6% of *Gpr83*$^{+}$ neurons (Figure S5G–I). Consistent with this expression analysis, hardly any tdTomato-labeled SPB neurons in *Calcrl*^{Cre};*Lbx1*^{FlpO};*Ai65*$^{ds\text{-}tdTom}$ mice expressed Tacr1 (Figure S5J–K), whereas almost all (96.0%) expressed Gpr83 (Figure S5L–M). Together, these data indicate that the *Calcrl*$^{+}$ SPB neurons are distinct from the *Tacr1*$^{+}$ population, and instead represent a subset of *Gpr83*$^{+}$ SPB neurons, which, unlike *Tacr1*$^{+}$ SPB neurons, receive inputs from low-threshold mechanosensory afferents and relay tactile information[29].

Mechanical and chemical itch are transmitted by distinct populations of SPB neurons

We then sought to assess how mechanical- and chemical-itch transmission are partitioned between different populations of molecularly defined SPB neurons. To do this, we examined expression of the immediate-early gene *cFos* in SPB neurons labeled by injection of the PBN with CTb or rAAV2-CAG-eGFP following either repetitive mechanical stimulation of the nape with a low-grade von Frey hair, or intradermal injection of histamine. cFos that was almost undetectable in SPB neurons in control mice (see Methods) but was frequently detected in SPB neurons throughout the dorsal horn and in the LSN following either mechanical or chemical itch treatment (Figure S6A–C). Strikingly, chemical itch-responsive SPB neurons were most frequently detected in lamina I, whereas mechanical itch-responsive SPB neurons were most frequently detected ventral to these neurons, in lamina IIo and lamina III (Figure S6D and E).

In *Calcrl*^{Cre};*Lbx1*^{FlpO};*Ai65*$^{ds\text{-}tdTom}$ mice, the majority (61.8%) of SPB neurons expressing cFos following mechanical-itch stimulation expressed tdTomato, whereas very few tdTomato^{+} SPB neurons responded to chemical itch treatment (6.1%) (Figure 3A–F), and these were located in the LSN. Similarly, nearly all (87.2%) mechanical itch-responsive

Author Manuscript Author Manuscript Author Manuscript Author Manuscript

neurons displayed Calcrl immunofluorescence, whereas very few (14.7%) chemical-itch responsive neurons exhibited Calcrl immunoreactivity (Figure 3G–L). Conversely, we never detected Tacr1 immunofluorescence in mechanical itch-responsive SPB neurons, but nearly all (92.7%) chemical itch-responsive neurons were Tacr1$^+$ (Figure 3M–R). Consistent with our hypothesis that the Calcrl$^+$ neurons that transmit mechanical itch represent a restricted subset of Gpr83$^+$ neurons, we detected Gpr83 expression in the majority (84.6%) of mechanical itch-responsive neurons, whereas relatively few (37.3%) chemical itch-responsive neurons expressed Gpr83 (Figure 3S–X). These data reveal a clear distinction between the SPB populations that transmit mechanical versus chemical itch and confirm that *Calcrl* defines a subset of SPB neurons that transmit mechanical itch. Interestingly, the distinction between mechanical- and chemical-itch responsiveness was less pronounced for the Gpr83$^+$ population, perhaps reflecting the partial overlap between the Tacr1$^+$ and Gpr83$^+$ SPB populations (Figure S5A–B).

To further investigate the functional distinction between Calcrl$^+$/Gpr83$^+$ neurons and Tacr1$^+$ neurons, we assessed mechanical- and chemical-itch responses following targeted ablation of the Gpr83$^+$ neurons and Tacr1$^+$ populations. Selective ablation of the spinal Tacr1$^+$ neurons by i.t. injection of substance P-saporin (SSP-SAP) (Figure S7A–K) failed to attenuate mechanical-itch responses (Figure S7M–N), as previously reported[3]. By contrast, injection of saporin conjugated to the Gpr83 ligand PEN peptide (PEN-SAP; see Methods) resulted in the loss of both Gpr83$^+$ and Calcrl$^+$ neurons from the dorsal horn (Figure S7G–L), which was accompanied by the loss of mechanical-itch sensitivity in wild type mice (Figure S7O) and mechanical itch-sensitized mice (Figures S7P–Q). Together, these data show that Gpr83$^+$ neurons transmit mechanical itch and corroborate our hypothesis that the Calcrl$^+$ neurons that transmit mechanical itch are a subset of Gpr83$^+$ SPB neurons.

A comprehensive assessment of chemical-itch transmission by SPB subpopulations that express either Tacr1 or Gpr83 using a battery of pruritogens determined to activate all three classes of pruriceptive neurons previously identified by single cell RNA sequencing[30–37] revealed that scratching responses to multiple pruritogens were dramatically reduced following Tacr1$^+$ neuron ablation (Figure S7R) but were unaffected by ablation of the Gpr83$^+$/Calcrl$^+$ neurons (Figure S7S). These findings show that the Tacr1$^+$/Gpr83$^-$ subdivision of SPB neurons relay all forms of chemical itch from the spinal cord to the brainstem, whereas mechanical itch is conveyed by the Calcrl$^+$/Gpr83$^+$/Tacr1$^-$ subdivision.

FoxP2^{PBN} neurons receive inputs from Calcrl^{Lbx1} SPB neurons

Our observation that Calcrl$^+$ SPB neurons terminate primarily within the dorsal PBN prompted us to identify their postsynaptic targets. The transcription factor FoxP2 marks one of two major divisions of excitatory neurons in the PBNsl, PBNdl, and PBNcl[38–41], leading us to ask if these neurons play a role in integrating mechanical-itch information relayed from the spinal cord to the PBN. Consistent with this, expression of synaptophysin-GFP in Calcrl^{Lbx1} neurons revealed an abundance of putative synaptic contacts from Calcrl^{Lbx1} neurons onto FoxP2-immunoreactive neuronal somata, particularly in the PBNsl and PBNdl (Figure 4A), To assess whether Calcrl^{Lbx1} SPB neurons directly innervate FoxP2^{PBN} neurons, whole-cell recordings were made from dorsal PBN neurons in acute brainstem

Author Manuscript Author Manuscript Author Manuscript Author Manuscript

slices from *Calcrl*^{Cr};*Lbx1*^{FlpO};*R26*$^{ds\text{-}ReaChR}$ mice, and FoxP2-expression by recorded neurons was determined by *post hoc* immunostaining (Figure 4C and D). Synaptic jitter in response to repetitive excitation of the Calcrl^{Lbx1} terminals was used to determine the location of neurons within the dorsal PBN receiving monosynaptic inputs from Calcrl^{Lbx1} SPB neurons[42,43]. Monosynaptic inputs, defined as having low (< 1 ms) synaptic jitter (mean: 0.50 ± 0.07 ms) with a low failure rate (0.06 ± 0.03), were detected in 54% of the recorded *FoxP2*$^{+}$ neurons (n = 42; Figure 4D–G). These *FoxP2*$^{+}$ neurons were located within the PBNsl and PBNdl, in a region that directly overlaps the location of Calcrl^{Lbx1} synaptophysin-GFP^{+} puncta. By contrast, very few FoxP2^{-} neurons received monosynaptic inputs from Calcrl^{Lbx1} terminals (n = 16). A further 31% of the FoxP2^{PBN} neurons were found to receive polysynaptic inputs, as defined by high (> 1 ms) synaptic jitter (mean 8.76 ± 2.88 ms) and a high failure rate (0.29 ± 0.05) (Figure 4E–G). In 5/5 neurons displaying low-jitter responses to stimulation of Calcrl^{Lbx1} terminals, of which 4/5 were FoxP2^{+}, synaptic inputs were blocked in the presence of tetrodotoxin, but restored following perfusion of 4-aminopyridine, which selectively reestablishes monosynaptic transmission (Figure 4H–I). Together, these results show that FoxP2^{PBN} neurons receive both direct monosynaptic and indirect polysynaptic inputs from ascending Calcrl^{Lbx1} SPB neurons.

FoxP2^{PBN} neurons mediate scratching in response to mechanical and chemical itch stimuli

In light of the demonstrated connectivity between the Calcrl^{Lbx1} SPB neurons and FoxP2^{PBN} neurons, we asked if the FoxP2^{PBN} neurons are required for protective scratching responses to mechanical itch. Administration of CNO to *FoxP2*^{Cre} mice following injection of AAV-Ef1a-DIO-hM4D(Gi)-mCherry into the PBN substantially reduced touch-evoked scratching in unsensitized mice (Figure 5A–B). Evoked and spontaneous scratching were also strongly reduced following disinhibition of the mechanical-itch pathway by blockade of Y1 receptors (Figures 5C). These results identify the FoxP2^{PBN} population as a key postsynaptic target of the Calcrl^{Lbx1} neurons that is required for conveying mechanical-itch information from the spinal cord to the PBN.

Because the PBN has been shown to be essential for the processing of chemical-itch information[11,12], we then asked whether FoxP2^{PBN} neurons are also required for the transmission of chemical itch. Scratching responses elicited by 48/80 or chloroquine were significantly reduced when the FoxP2^{PBN} neurons were silenced (Figures 5D–E), indicating that FoxP2^{PBN} neurons are required for behavioral responses to histaminergic and non-histaminergic itch, respectively.

This finding prompted us to assess whether FoxP2^{PBN} neurons receive inputs from the Tacr1^{+} SPB neurons that transmit chemical itch in addition to the Calcrl^{Lbx1} afferents that transmit mechanical itch. To profile inputs to FoxP2^{PBN} neurons, we performed monosynaptic retrograde tracing from FoxP2^{PBN} neurons (see Methods). One week following bilateral injection of the PBN with EnvA-pseudotyped, ΔG-mCherry rabies virus (Figure 5F), mCherry^{+} cells could be seen in laminae I-IIo, lamina V and the LSN in cervical segments of the spinal cord (Figure 5G–J), as well as in supraspinal regions implicated in itch responses, namely the somatosensory cortex, amygdala and PAG[19,44–46] (Figure S8A–C). Within the spinal cord, the majority of mCherry^{+} neurons displayed Tacr1

Author Manuscript Author Manuscript Author Manuscript Author Manuscript

immunoreactivity (74.8 ± 0.3%) (Figure 5G and 5J), consistent with reports that the majority of SPB neurons express Tacr1[24,29]. In addition, a substantial fraction co-expressed Calcrl (Figure 5H and 5J) (66.6 ± 7.5%) or Gpr83 (Figure 5I and 5J) (56.0 ± 4.4%). These data reveal marked by FoxP2^{PBN} neurons receive both mechanical- and chemical-itch information from the spinal cord.

Mechanical and chemical itch are transmitted by separate pathways within the PBN

In vivo calcium imaging by fiber photometry was used to monitor the calcium dynamics of FoxP2^{PBN} neurons during touch-evoked scratching. Following injection of AAV-DIO-GCaMP7s-WPRE into the PBN of *FoxP2^{Cre}* mice (Figure 6A), calcium signals from FoxP2^{PBN} neurons were selectively assessed during episodes of hindlimb scratching evoked by stimulation of the nape with a 0.07g von Frey hair. A significant time-locked elevation of calcium in FoxP2^{PBN} neurons was recorded, with the initial responses occurring immediately after nape stimulation but before scratching onset (Figure 6B–E). These data indicate that the increase in neural activity in FoxP2^{PBN} neurons both precedes and predicts the onset of scratching and indicate that the FoxP2^{PBN} neurons are activated by mechanical-itch stimuli, consistent with their role in generating protective hindlimb scratching.

To determine whether the central transmission pathways for mechanical- and chemical-itch converge supraspinally at the level of FoxP2^{PBN} neurons, or remain segregated, we performed miniature microendoscopy to monitor *in vivo* calcium activity of the FoxP2^{PBN} neurons at the single-cell level during mechanical- and chemical-itch stimulation (Figure 6F–G). 35 out of 189 recorded cells (n = 5 mice) responded to either mechanical or chemical itch of which 37.1% were selectively tuned to mechanical-itch stimulation (Figure 6H–J and 6M) and 60.0% responded only to chemical stimulation (Figure 6H–I, 6K and 6M). Only 2.9% (1 out of 35) of itch-responsive neurons were activated by both mechanical and chemical stimuli (Figure 6H–I and 6L–M), indicating the FoxP2^{PBN} population comprises two discrete subsets of neurons, each mediating either mechanical or chemical itch.

Concurrent recruitment of mechanical and chemical itch pathways in models of pruritis

Chronic itch is characterized by persistent spontaneous itch, as well as hypersensitivity to mechanical-itch stimuli (hyperknesis) and innocuous tactile stimuli that typically do not cause itch (alloknesis). This mechanical hypersensitivity contributes to a cycle of itching, scratching and inflammation that exacerbates and perpetuates the underlying condition[47]. In chronic itch, the pathways for acute mechanical and chemical itch in the periphery and spinal cord are dysregulated, suggesting that the processing of itch by supraspinal centers is likewise disrupted[11]. Toa ssess the contribution that molecularly defined SPB neurons make to hyperknesis/alloknesis and spontaneous scratching under chronic-itch conditions, and to hyperknesis/alloknesis in acute pruritis, we examined the role of the Calcrl^{Lbx1} neurons in a mouse model of allergic contact dermatitis[48]. These mice exhibit both spontaneous scratching and hypersensitivity to punctate mechanical itch stimuli delivered by low-grade (0.07 g) von Frey-hair stimulation to the region surrounding the treated area of skin, both of which were strongly reduced following ablation of the Calcrl^{Lbx1} neurons (Figure 7A). Ablation of the Gpr83^{+} fraction of SPB neurons also reduced hyperknesis/alloknesis and spontaneous scratching in these mice (Figure 7B). Hyperknesis/alloknesis and spontaneous

Author Manuscript Author Manuscript Author Manuscript Author Manuscript

scratching were also reduced following ablation of the Tacr1^{+} fraction of SPB neurons that transmit acute chemical itch (Figure 7C). When the contribution of SPB populations to hyperknesis/alloknesis and spontaneous scratching was assessed in a mouse model of dry skin itch[49,50], we again observed a marked reduction in itch responses following ablation of the Calcrl^{Lbx1} neurons, Gpr83^{+} neurons or Tacr1^{+} neurons (Figures 7D–7F). Together these data show that, in chronic itch, functionally segregated SPB populations that normally transmit either acute mechanical or acute chemical itch are concurrently recruited, with both pathways contributing to spontaneous itch as well as tactile hypersensitivity. Moreover, hM4D-dependent silencing of the FoxP2^{PBN} neurons reduced hyperknesis/alloknesis and spontaneous scratching in allergic contact dermatitis mice, demonstrating that chronic-itch signals converge on and are mediated by *FoxP2*$^{+}$ neurons in the dorsal PBN (Figure 7H).

To further investigate the contribution the supraspinal pathways for mechanical- and chemical-itch transmission make to the development of pruritis, we employed a model of acute hyperknesis/alloknesis in which injection of histamine into the nape causes hypersensitivity to punctate stimuli delivered by a low-grade (0.07 g) von Frey hair to the area of skin surrounding the injection site[51]. This hypersensitivity was abrogated by loss-of-function manipulations of the supraspinal transmission pathway for mechanical itch, either by silencing the Calcrl^{Lbx1} SPB neurons (Figure 8A), or by ablation of the Gpr83^{+} neurons (Figure 8B), indicating that alloknesis entails elevated activity in this pathway. Interestingly, ablation of the Tacr1^{+} neurons that constitute the supraspinal pathway for chemical-itch transmission also reduced hyperknesis/alloknesis responses (Figure 8C), as did i.t. injection of the Tacr1 antagonist CP 96345 (Figure 8D), indicating that central activation of the chemical-itch pathway is a necessary condition of hyperknesis/alloknesis. To test whether it is also a sufficient condition of hyperknesis/alloknesis, we assessed itch responses following direct activation of Tacr1^{+} neurons. Upon i.t. delivery of the selective Tacr1 agonist [Sar^{9}, Met(O$_2$)^{11}]-substance P (SSP), mice displayed hypersensitivity to low-threshold stimulation of the nape in addition to spontaneous scratching (Figure 8E). Thus, central activation of the chemical itch pathway, including the neurons that transmit chemical itch supraspinally, is both necessary and sufficient for hyperknesis/alloknesis. Finally, silencing the *FoxP2*$^{+}$ neurons in the dorsal PBN also attenuates hyperknesis/alloknesis following intradermal histamine injection (Figure 8F) indicating that acute hyperknesis/alloknesis, like chronic itch, is mediated by the convergent signaling of the mechanical- and chemical-itch pathways on FoxP2^{PBN} neurons in the dorsal PBN.

DISCUSSION

This study identifies an essential spinoparabrachial pathway for mechanical-itch transmission that is required for scratching in intact mice. We find that mechanical and chemical itch are transmitted as distinct modalities along the length of the neuraxis to the PBN, where discrete subsets of *FoxP2*$^{+}$ neurons engage a common motor program in response to both acute mechanical and chemical itch. Notably, dysregulated transmission along both the mechanical- and chemical-itch pathways results in pathological chronic itch, arguing that these pathways act cooperatively in the genesis of chronic itch. Finally, our demonstration that the mechanical itch-scratch motor program is regulated at the level of the

Author Manuscript Author Manuscript Author Manuscript Author Manuscript

PBN implies that the mechanical-itch SPB-PBN pathway assigns a noxious valence to an otherwise-innocuous tactile stimulus.

$Calcrl^{Lbx1}$ SPB neurons constitute an essential spinofugal pathway for mechanical itch

The spinoparabrachial projection neurons that transmit mechanical-itch information are derived from *Lbx1*-expressing dorsal-horn somatosensory neurons[52,53] that express the CGRP receptor subunit Calcrl. This $Calcrl^{Lbx1}$ SPB population represents a more stringent division of SPB neurons than those previously described by Choi et al. (2020). Our results demonstrate a sharper molecular (Figure S5) and functional distinction (Figure 3) between the $Calcrl^{+}$ and $Tacr1^{+}$ SPB populations than between the $Gpr83^{+}$ and $Tacr1^{+}$ populations. We therefore propose that mechanical itch is transmitted from the spinal cord to the PBN along an *Calcrl*$^{+}$/*Lbx1*$^{+}$ SPB pathway that comprises a subset of the $Gpr83^{+}$ neurons that do not express Tacr1. By contrast, the $Tacr1^{+}$ SPB neurons are recruited after chemical-but not mechanical-itch stimulation (Figure 3) and they appear to transmit chemical- and chronic-itch information selectively, based on the observed reduction in scratching under these conditions following ablation of spinal $Tacr1^{+}$ neurons[3,54]. The interpretation of these studies is, however, confounded by the recent finding that Tacr1 is expressed in some spinal $Grpr^{+}$ interneurons[11,55] that have an established role in chemical-itch transmission[5,6].

Our determination that the SPB neurons that transmit chemical itch are $Tacr1^{+}/Gpr83^{-}$ does not eliminate the possibility that $Tacr1^{+}$ population comprises subpopulations that are selective for different chemical-itch stimuli, as anterolateral projection neurons in primates are differentially sensitive to histaminergic and non-histaminergic pruritogens[56–58]. In contrast to the $Calcrl^{Lbx1}$ neurons that transmit mechanical itch and selectively innervate the PBN, a subset of SPB neurons that respond to pruritogens project to the thalamus[59], suggesting the *Tacr1*$^{+}$ neurons may also be functionally heterogeneous. The Tacr1 ligand tachykinin 1 (Tac1) is also expressed in a subpopulation of *Lbx1*-derived neurons that project to both the PBN and thalamus[60], with ablation of these $Tac1^{Lbx1}$ neurons impairing histaminergic and non-histaminergic itch[60], but not mechanical itch. This suggests Tac1 and Tacr1 define a subset of SPB neurons that transmit some forms of chemical itch. However, because the $Tac1^{Lbx1}$ population of dorsal horn neurons also includes spinal interneurons, the precise role of $Tac1^{+}$ SPB neurons in chemical-itch transmission remains to be determined.

The PBN is essential for the supraspinal processing of mechanical and chemical itch

Our demonstration that scratching evoked by mechanical itch is driven by information transmitted through and regulated by the PBN (Figures 5 and 6) is consistent with previous studies indicating that the PBN constitutes the primary supraspinal recipient nucleus for ascending noxious somatosensory information[23,24]. Whereas prior studies showed the PBN functions to coordinate protective behavioral responses to aversive stimuli elicited by high-threshold mechanoreceptors and chemical pruritogens[11,12,60], we now show the PBN is required for scratching elicited by short-lived low-threshold tactile stimuli that are typically not perceived as noxious.

Author Manuscript Author Manuscript Author Manuscript Author Manuscript

FoxP2-expressing parabrachial neurons located in the PBNsl, PBNdl, and PBNcl[38–40] can be functionally subdivided into populations that receive either mechanical- and chemical-itch information (Figure 6), and these neurons are required for implementing the itch-scratch motor program following either mechanical- or chemical-itch stimulation. Interestingly, the FoxP2^{PBN} neurons correspond to one of two developmentally distinct macropopulations of glutamatergic neurons within the PBN, with those expressing *Atoh1* rather than *Lmx1a/b* being further distinguished by their dorsal location and connectivity[41]. Our study reveals a novel level of functional diversity within the FoxP2 population and paves the way for future work to distinguish the subsets of FoxP2^{+} neurons that mediate each form of itch with respect to their detailed molecular identity, location and connectivity.

Chemical itch is known to activate multiple brain regions that are innervated by the PBN, including those associated with aversive valence, stress, threat and motor planning[14–18], with transmission to these regions presumably underlying the sensory-discriminative, affective-motivational and cognitive components of itch sensation[13]. Less is known about the role of these brain regions in mechanical itch; however, the observations that: 1) mechanical and chemical stimuli elicit identical motivational and motor behaviors, 2) both modalities are transmitted to *FoxP2*$^{+}$ neurons in the dorsal PBN, and 3) scratching responses to multiple itch modalities are abolished when FoxP2^{PBN} neurons are silenced, strongly indicate the FoxP2^{PBN} neurons coordinate a range of protective strategies, including site-directed scratching and avoidance behaviors[18–20].

Furthermore, these observations are consistent with a model whereby the PBN, rather than acting solely as a waystation for itch information, instead integrates multiple streams of information about affective-behavioral states and the external environment, to select context-appropriate protective behaviors[12,61,62]. Consistent with this hypothesis of context-dependent action selection, activation of a pain transmission pathway within the PBN suppresses scratching in response to chemical itch[63]. This suppression of itch by a painful counterstimulus might function to permit animals to attend to a more urgent threat, or perhaps prevent damage to the skin by scratching[13,58,64].

Supraspinal processing is essential for normal protective responses to itch

The suppression of scratching that occurs following loss-of-function manipulations targeting either the PBN (this study; references 11 and 12) or select populations of spinofugal neurons (this study; references 65 and 66) together with classical descriptions of the scratch reflex in spinalized animals[9,10,67–69] are consistent with strong descending tonic inhibition of itch-driven scratching, which is then alleviated upon activation of the PBN by SPB neurons. Such a mechanism would be ideally suited to facilitate the gating of reflexive scratching in a context- or state-dependent manner. In support of this hypothesis, the PBN sends inputs to several supraspinal areas that are implicated in the descending modulation of itch[19,44,76,45,46,70–75]. Perhaps most saliently, FoxP2^{PBN} neurons project directly to the PAG[73], which in turn acts via descending pathways originating in the RVM to exert bidirectional control over spinal pathways for itch and pain. Pruritogens elicit or suppress activity in separate populations of PAG neurons[44], and scratching is suppressed by activation of GABAergic neurons or inhibition of glutamatergic neurons in the PAG[45]. Conversely,

Author Manuscript Author Manuscript Author Manuscript Author Manuscript

a population of glutamatergic neurons that project from the PAG to the RVM is required for itch-induced scratching[44]. Moreover, glutamatergic neurons within the RVM project to the dorsal horn of the spinal cord, which when activated cause scratching in a manner at least partly dependent on the $Grpr^+$ neuronal pathway[44]. By contrast, selective activation of GABAergic ON cells within the RVM, so called because they are activated by algogenic stimuli, inhibits chemical itch as well as spontaneous itch and alloknesis in a chronic itch model, while facilitating pain responses[72]. Although the modulation of mechanical itch by the PAG-RVM-spinal cord axis is yet to be investigated, the modulation of all forms of itch by a common descending pathway would represent an efficient strategy for selecting itch behaviors in response to affective motivation[45].

Our observation that *FoxP2*$^+$ neurons in the dorsal PBN receive inputs from S1, CeA and the PAG (Figures S8A–S8C) raises the possibility that the *FoxP2*$^+$ neurons in the dorsal PBN contribute to scratch action selection by integrating information from these regions with incoming itch signals from the spinal cord. We propose that scratch action selection is in turn mediated by $Calca^+$ neurons in the PBNel, which have been shown to drive scratching responses to chemical pruritogens[12]. Although our findings indicate that the $Calcrl^{Lbx1}$ SPB neurons do not directly innervate PBN_{el} (Figure 2B), the *Calca*$^+$ neurons in the PBNel are likely to be positioned downstream of *FoxP2*$^+$ neurons. Notably, the *Calca*$^+$ neurons send projections to the PAG, amygdala, thalamus and medulla[74], all of which modulate itch behaviors[19,44,45,76].

Separate transmission pathways for mechanical and chemical itch are both recruited in pathological itch

The observation that mechanical and chemical itch are experienced as a similar sensation that drives a common protective response (scratching), have promted the hypothesis that the mechanical- and chemical-itch transmission pathways converge on a common neuronal pathway either within the spinal cord or downstream of spinal projection neurons[3,77]. Our findings instead argue that acute mechanical and chemical itch are transmitted along labeled lines across several synapses from the PNS to the PBN[78,79]. Mechanical-itch transmission in the PNS is mediated by Aß low-threshold mechanoreceptors (LTMRs) that express Toll-like receptor 5[2] and in the dorsal horn by neurons that express Ucn3::Cre[2] and Y1[3]. Ablating these populations fails to affect chemical itch, while ablation of *Grpr*$^+$ neurons that transmit chemical itch fails to attenuate mechanical-itch transmission[2–4] (however, see reference 77). Mechanical and chemical itch are also separated within the ascending pathways to the PBN, and within the PBN at the level of the $FoxP2^{PBN}$ neurons that receive inputs from the *Calcrl*$^+$ and *Tacr1*$^+$ subpopulations of SPB neurons. Together, these findings raise the possibility that acute mechanical and chemical itch represent distinct modalities at all stages of neural processing.

The differential sensitivity of these pathways to modulation by different populations of spinal inhibitory interneurons, namely the BI-5 neurons for chemical itch and the NPY^{Lbx1} INs for mechanical itch[4,7], suggests the separation of these pathways may permit the stimulus-specific modulation of mechanical and chemical itch at multiple levels of processing by feedforward[4,64,80] and descending[46] mechanisms. Within the PBN, the

Author Manuscript Author Manuscript Author Manuscript Author Manuscript

processing of acute mechanical- and chemical-itch information by distinct populations of neurons would also enable the differential integration of information from other supraspinal regions to facilitate protective responses appropriate to the nature of the stimulus in a context- or state-dependent manner.

Implications for Chronic Itch

Our results indicate that the distinction between the mechanical- and chemical-itch pathways becomes blurred in pathological itch. In chronic itch, the spinofugal pathways for both acute mechanical and chemical itch are persistently hyperactivated, such that the ablation of either pathway relieves mechanical hypersensitivity and spontaneous itch (Figure 7). This is consistent with the dysregulation of the mechanical- and chemical-itch pathways within the skin and spinal cord in a range of chronic itch models[2,44,77,81]. Likewise, in acute hyperknesis/alloknesis, pruritogens sensitize the region of skin surrounding the treated area to mechanical stimuli[51,65]. This sensitization is mediated centrally, as activating the *Tacr1*$^{+}$ neurons that form the chemical itch pathway is sufficient to induce hyperknesis/alloknesis, whereas their loss prevents hyperknesis/alloknesis (Figure 8). This mechanism likely underlies hypersensitivity to mechanical stimuli in chronic-itch conditions where infiltration of the epidermis by immune cells results in persistent elevation of pruritogens such as histamine and enduring activation of the chemical-itch pathway[31,82,83].

In summary, this study identifies the key populations of projection neurons that transmit mechanical-versus chemical-itch signals from the spinal cord to the PBN, and it demonstrates that the labeled-line transmission of acute mechanical and chemical itch extends from the periphery into the brainstem. This segregation of transmission is disrupted in chronic itch, with the central facilitation of mechanical-itch transmission by activity within the chemical-itch pathway being a key driver of pathological itch. We propose that the FoxP2^{PBN} neurons function as a nexus between the spinal reflex circuitry for itch and the supraspinal circuitry that encodes context, thereby enabling external sensory information to be synthesized with internal state information to ensure that protective scratching behaviors are generated in a context-appropriate manner.

STAR METHODS

RESOURCE AVAILABILITY

Lead Contact—Further information and requests for resources and reagents should be directed to Martyn Goulding (goulding@salk.edu).

Materials Availability

All published reagents and mouse lines will be shared upon request within the limits of the respective material transfer agreements.

Data and Code Availability

This study did not generate new datasets or codes.

Author Manuscript Author Manuscript Author Manuscript Author Manuscript

EXPERIMENTAL MODEL AND SUBJECT DETAILS

All protocols for animal experiments were approved by the IACUC of the Salk Institute for Biological Studies according to NIH guidelines for animal experimentation. Male and female mice were used in all studies. Animals were randomized to experimental groups and no sex differences were noted.

The following mouse lines were also used in this study: *Calcrl*^{Cre}[26], *FoxP2*^{Cre}[84], *NPY::Cre*[4], *Lbx1*^{FlpO}[4], *Cdx2::FlpO*[25], *Ai14*$^{lsl\text{-}tdTom}$[85], *Ai65*$^{ds\text{-}tdTom}$[86], *R26*$^{ds\text{-}Syp}$ *(RC::FPSit)*[87], *R26*$^{ds\text{-}hM3D}$[88], *R26*$^{ds\text{-}hM4D}$[4], *R26*$^{ds\text{-}ReaChR}$[89], *Tau*$^{ds\text{-}DTR}$[25].

METHOD DETAILS

Immunohistochemistry

The following primary antibodies were used in this study: rabbit α-Calcrl (1:50; Invitrogen), mouse α-cFos (1:500; Abcam), goat α-CTB (1:4000; List Laboratories), rabbit α-DsRed (1:1000; Clontech), rabbit α-FoxP2 (1:500; Sigma), chicken α-GFP (1:000; Aves), rabbit α-Gpr83 (1:500; Alomone Labs), chicken α-LacZ (1:1000; Abcam) rabbit α-NK1R (1:500; Advanced Targeting Systems), mouse α-PSD95 (1:500; Millipore), rat α-RFP (1:1000; Chromotek).

Mice were euthanized by a single intraperitoneal (i.p.) injection (10 µl g^{-1} body weight) of ketamine (10 mg ml^{-1}) and xylazine (1 mg ml^{-1}) immediately prior to perfusion with 20 ml ice-cold 4% paraformaldehyde (PFA) in PBS. Except for those used for patch-clamp recordings (see below), all tissues were dissected and post-fixed for 1 h at RT, then washed 3 times in PBS and cryoprotected in 30% sucrose-PBS (w/v) overnight at 4 °C before being embedded in Tissue-Tek OCT Compound (Sakura Finetek) and cryosectioned at 30 µm. For histological analysis, sections were dried at RT and stored at −20 °C. Sections were washed once with PBS (5 min), blocked with a solution of 10% donkey serum in PBT (PBS, 0.1% Triton X-100) for 1 h at RT and then incubated overnight at 4 °C with primary antibodies in a solution of 1% donkey serum in PBT. Sections were then washed 3 times (15 min each) in PBT before being incubated for 2 h at RT with fluorophore-conjugated secondary antibodies (1:1000; Jackson Laboratories) in a solution of 1% donkey serum in PBT. Sections were then washed 3 times (15 min each) in PBT. Some sections were then incubated with NeuroTrace 435/455 (Invitrogen) at 1:300 in PBT before being washed once in PBT and mounting in Aqua-Poly/Mount (Polysciences).

For identification of biocytin-filled cells following electrophysiological recording, free-floating sections were incubated in PFA overnight at 4 °C. Sections were washed three times with PBS (15 min each), blocked with a solution of 10% donkey serum in PBT (PBS, 0.1% Triton X-100) overnight at 4 °C, and then incubated overnight at 4 °C with primary antibodies in a solution of 1% donkey serum in PBT. Sections were then washed 3 times (15 min each) in PBT before being incubated overnight at 4 °C with streptavidin-Cy5 (1:50; Invitrogen) and fluorophore–conjugated secondary antibodies (1:1000; Jackson Laboratories) in a solution of 1% donkey serum in PBT. Sections were again washed 3 times (15 min each) in PBT before being mounted with Aqua-Poly/Mount (Polysciences).

Author Manuscript Author Manuscript Author Manuscript Author Manuscript

A Zeiss LSM 700 confocal microscope was used to capture images. ImageJ software was used to assess immunofluorescence, with thresholds set according to signal intensity[90].

RNA Fluorescence *In Situ* Hybridization

For RNAscope RNA FISH, the following probes were used: EGFP-sense-C2, Mm-Calcrl, Mm-Calcrl-C3, Mm-Gpr83, Mm-Tacr1-C3 (Advanced Cell Diagnostics). These were revealed with Opal 520, Opal 520, Opal 650 (PerkinElmer).

Tissue was prepared as described above for immunohistochemistry and cryosectioned at 14 μm. Multiple-labeling fluorescence *in situ* hybridization was performed using the RNAscope Multiplex Fluorescent Reagent Kit v2 Assay (Advanced Cell Diagnostics) following the manufacturer's recommended protocol. Sections were mounted using SlowFade Gold Antifade Reagent with DAPI (Invitrogen) and imaged under a 40x oil objective on a Zeiss LSM700 confocal microscope. For quantification, multiple sections from each spinal cords were analyzed per condition, in order to identify $eGFP^{+}$ SPB neruons, and only cells with clearly visible nuclei were scored.

cFos Induction

cFos induction protocols were performed 3 weeks after rAAV2-CAG-eGFP injection and 1 week after CTb injection. For mechanical itch stimulation, mice were placed in a plexiglass chamber and a 0.7 g von Frey hair was repeatedly applied to the nape for 1 s at an interval of 30 s for 30 min. For chemical itch stimulation, mice received an i.d. injection of histamine (100 μg in 50 μl) into the nape before being placed in a plexiglass chamber. For mechanical-itch controls, mice were placed in the plexiglass chamber without von Frey hair stimulation. For chemical-itch controls, mice received an injection of sterile saline (0.9%, 50 μl) instead of histamine. Following the initial stimulation/control treatment, mice remained in the chamber for 90 min before perfusion and tissue collection.

Stereotaxic Surgery—For each surgery, mice were anesthetized with isoflurane (4% for induction, 1.5 to 2 % for maintenance with a nose cone; Dräger Vapor 2000, Draegar, Inc.) and kept on a heating pad throughout the surgery. Each mouse was then placed on a stereotaxic frame (David Kopf Instruments), the skull exposed, and the cranium drilled with a high-speed stereotaxic drill (Model 1474, David Kopf Instruments). To systemically target PBN_L neurons, the following coordinates were used: antero-posterior (AP), −5.20mm from Bregma; medio-lateral (ML), ±1.50 mm; dorsoventral (DV), −3.40 mm. To systemically target DCN neurons, the following coordinates relative to obex were used. For the cuneate nucleus, site 1: AP, 0.00 mm; ML, ±0.70 mm; DV, −0.40 mm; site 2: AP, 0.25 mm; ML, ±0.85 mm; DV, −0.40 mm; site 3: AP, 0.48 mm; ML, ±1.00 mm; DV, - 0.40 mm. For the gracile nucleus, site 1: AP, −0.25 mm from Obex; ML, ±0.25 mm; DV, −0.20 mm; site 2: AP, 0.00 mm; ML, ±0.25 mm; DV, −0.20 mm; site 3: AP, 0.25 mm; ML, ±0.45 mm; DV, - 0.20 mm. For the cell-type specific targeting of $FoxP2^{PBN}$ neurons, injections were made into the PBN_L: AP, −1.00 mm from lambda; ML, ±1.50 mm; DV, −3.25 mm.

Viruses were administered with a glass pipette (tips broken for an inner diameter of 20 μm) connected to a Nanoject III Programmable Nanoliter Injector (Drummond Scientific)

Author Manuscript Author Manuscript Author Manuscript Author Manuscript

at a rate of 60 nl min^{-1}. For drug infusion, a bilateral micro-cannula set (P1 Technologies), including guide cannula (C235G, 3.0mm C/C, P1 Technologies), dummy cannula (C235DC, P1 Technologies) and dust cap (303DC/1A, P1 Technologies), was implanted into the PBN_L (AP, −1.00 mm from lambda; ML, ±1.50 mm; DV, 3.20 mm). The implants were covered with superglue and dental cement for stabilization.

Viral Injections—For systemic PBN silencing, wild type mice were bilaterally injected with 400 nl AAVDJ-hSyn-HA-hM4D(Gi)-mCherry (3.11E+13 GC ml^{-1}, Salk Institute Viral Vector Core) or AAVDJ-CMV-eGFP (1.35E+13 GC ml^{-1}, Salk Institute Viral Vector Core) into PBN_L. To silence the DCN, wild type mice were bilaterally injected with 50 nl AAVDJ-hSyn-HA-hM4D(Gi)-mCherry into each injection spot (300 nl in total each side). For cell-type specific silencing of $FoxP2^{PBN}$ neurons, *FoxP2*^{Cre} mice were bilaterally injected with 350 nl AAVDJ-EF1a-DIO-hM4D(Gi)-mCherry (6.04E+11 GC ml^{-1}, Salk Institute Viral Vector Core) or AAVDJ-Syn1-DIO-eGFP (2.31E+12 GC ml^{-1}, Salk Institute Viral Vector Core) into PBN_L. For retrograde tracing, *Calcrl*^{Cre}; *Lbx1*^{FlpO}; *Ai65*^{dsTom} mice or wild type mice were bilaterally injected with 500 nl rAAV2-CAG-eGFP (3.25E+12 GC ml^{-1}, from Y. Liu) or cholera toxin subunit B conjugated to Alexa Fluor 647 (CTb; Invitrogen) into PBN_L.

Fiber photometry—For fiber photometry, the PBN_L of *FoxP2*^{Cre} mice was injected with 350 nl AAV1-hSyn-DIO-jGCaMP7s (Addgene viral prep 104491-AAV1) (3.75E+13 GC ml^{-1}) or control AAV1-hSyn-DIO-eYFP (2.12E+12 GC ml^{-1}). A stainless-steel mono fiberoptic cannula (400-μm diameter, NA 0.37, Doric Lenses) was then implanted using the coordinates listed above for cannula implantation. The implants were covered with superglue and dental cement for stabilization.

A 1-site Fiber Photometry System, 405 and 465 nm (Doric Lenses Inc, Canada) was used to record activity in $FoxP2^{PBN}$ neurons. GCaMP isosbestic fluorescence (405-nm excitation) and calcium-dependent fluorescence (465-nm excitation) were recorded at a sampling rate of 12 kHz, and data were analyzed with Doric Neuroscience Studio software. F0 was calculated by a least mean squares fitting of the 405 nm channel relative to the 465 nm channel, and ΔF/F was calculated as (F465-F405_fitted)/F405_fitted. Data were further analyzed with custom MATLAB scripts.

In vivo single cell calcium imaging

An Inscopix nVista 2 miniature microendoscope (miniscope) was used to record calcium activities at 10 Hz and 0.4–1 mW/mm^2 LED power. Animals were habituated following attachment of the miniscope in the itch-testing chambers for 2 days (30-60 min/day) before the recording day. On the recording day, animals were allowed to explore the home cage freely for 15 min while calcium activity and behavior were recorded. Mechanical-itch stimuli were given to the nape of the mice with a 0.07 g von Frey filament at a minimal interval of 30s. For chemical itch stimulation, chloroquine (200 mg in 50 ml) was injected intradermally into the nape of mice immediately before recording. A Raspberry Pi camera was used to trigger calcium recordings and record induced scratching episodes. Scratching onsets were determined from the recorded behavioral videos.

Author Manuscript Author Manuscript Author Manuscript Author Manuscript

Imaging data was preprocessed by the Inscopix data processing software with 2x spatial downsampling, correction of defective pixels, spatial band-pass filtering, and motion correction using the first frame as the global reference frame. Single-cell ROIs were identified by the CNMFe algorithm with post hoc manual validation. The output was measured as dF over noise and z-scored throughout the entire trace.

To delineate the heatmap, representative averaged calcium signals for each individual cell were plotted for mechanical- and chemical-itch stimulations, respectively. Cells were sorted by the average value in the mechanical or chemical itch trials and were plotted in the same order. To identify cells that responded to itch stimuli, the maximum or minimum values from −5 to +10 s around the scratching onset were calculated for each episode and “pre” and “post” groups were compared with paired t-tests. Neurons that showed significant differences in the statistical tests were classified as itch responsive.

Rabies Tracing

For rabies retrograde tracing, bilateral injections of 350 nl AAV1-hSyn-FLEX-TVA-P2A-eGFP-2A-oG (9.22E+11 GC ml^{-1}, Salk Institute Viral Vector Core) were made into PBN_L of *FoxP2*^{Cre} mice. After 3 weeks, mice received bilateral injections into the same area of 400 nl EnvA G-deleted rabies-mCherry (5.0E+07 GC ml^{-1}, Salk Institute Viral Vector Core). Mice were perfused 7 days after the rabies injection.

Cell Ablation—For intersectional ablation experiments, *NPY::Cre;Lbx1*^{FlpO}*;Tau*$^{ds\text{-}DTR}$*; Ai65*$^{ds\text{-}tdTom}$ mice were injected twice with diphtheria toxin (DT; 50 ng g^{-1} in 0.9% sterile saline, i.p.; List Biological Laboratories) at an interval of three days[4]. *Calcrl*^{Cre}*;Lbx1*^{FlpO}*;Tau*$^{ds\text{-}DTR}$*; Ai65*$^{ds\text{-}tdTom}$ and *Calcrl*^{Cre}*;NPY::Cre;Lbx1*^{FlpO}*;Tau*$^{ds\text{-}DTR}$*;Ai65*$^{ds\text{-}tdTom}$ mice received three intrathecal (i.t.) injections of DT (10 ng in 10 μl 0.9% sterile saline; List Biological Laboratories) at an interval of two days [91]. Spontaneous and evoked scratching in NPY^{Lbx1} IN-ablated mice were assessed 10 days following the first DT injection. For all other experiments, behavioral testing was performed 14-21 days following the first injection; controls were littermates of experimental animals and had identical genotypes but received injections of 0.9% sterile saline instead of DT.

For ablations using saporin-conjugated receptor ligands, P28 mice were given a single i.t. injection of PEN-saporin (PEN-SAP; 3 μg in 10 μl 0.9% sterile saline) to ablate $Gpr83^+$ neurons or [Sar^9, $Met(O_2)^{11}$]-substance P-saporin neurons (SSP-SAP; 100 ng in 10 μl 0.9% sterile saline; Advanced Targeting Systems)[3,92] to ablate $Tacr1^+$ neurons. PEN-SAP was produced by CytoLogistics (Carlsbad, CA) by biotinylation of PEN peptide, the endogenous ligand of Gpr83, followed by incubation with streptavidin-ZAP (Advanced Targeting Systems)[93,94]. Littermate controls received injections of an equal mass of blank saporin (Advanced Targeting Systems) in 10 μl 0.9% sterile saline. Behavioral testing and assessment of ablation efficiency by immunohistochemistry were performed 14 days later.

Inflammatory Pain Induction—To induce inflammatory pain, mice were briefly anesthetized with isofluorane (3–5 min at 2%), and 20 μl Complete Freund’s Adjuvant (CFA, Sigma) was injected into the plantar surface of the left hindpaw. Responses to static

Author Manuscript Author Manuscript Author Manuscript Author Manuscript

touch, dynamic touch and radiant heat were measured immediately before (day 0), 1 day and 3 days after CFA treatment.

Drug Administration

Mice were briefly anesthetized with 2.5% isoflurane in O_2 prior to i.t. injections. A 30-gauge needle was inserted into the fifth intervertebral space until it elicited a tail flick. The needle was held in place for 30 s and turned 90° prior to withdrawal to prevent outflow.

Clozapine *N*-oxide (CNO; Sigma) the Y1 receptor antagonist BIBP 3226 (Tocris), and CP 96345 (Tocris) were dissolved in DMSO, which was then diluted with 0.9% sterile saline so that the concentration of DMSO did not exceed 1% in injected solutions. [Sar^9, $Met(O_2)^{11}$]-substance P (SSP; Tocris) was dissolved in 0.9% sterile saline. CNO was administered by i.p. injection at 2 mg kg^{-1}. For cannulated mice, CNO (500 ng in 500 nl) was bilaterally infused into the PBN by a syringe drive system (BASi Research Products) at 112 nl min^{-1}. Cannulated mice were tested 10-15 min following administration. BIBP 3226 (5 μg in 10 μl)[3], CP 96345 (20 μg in 10 μl)[95] and SSP (25 pmol in 10 μl)[96] were administered by i.t. injection. Mice were tested 15-45 min following administration.

Electrophysiology

8-12-week-old mice were anaesthetized by i.p. injection of urethane (10 μl g^{-1}) and transcardially perfused with oxygenated ice-cold dissecting/slicing artificial cerebrospinal fluid (aCSF). A vibratome (Leica VT1000S) was used to cut 250-μm coronal brainstem slices in ice cold dissecting/slicing aCSF. Slices were then allowed to recover for 30 min in recording ACSF at 34°C and then for at least 1 h at RT prior to recording. Signals from patch-clamp electrodes (6-10 MΩ) were amplified and filtered (4 kHz low-pass Bessel filter) with a MultiClamp 700B amplifier (Molecular Devices) and acquired at 50 kHz with a Digidata 1440A A/D board and pCLAMP software (Molecular Devices). For ReaChR-mediated stimulation of projection neuron terminals, a single LED optic fiber source (~2 mW output at 591 nm) was positioned ~10 mm from the surface of the slice, illuminating its entire surface. 5-10 stimuli were delivered at 5 Hz with a 10-ms pulse width. All drugs were bath applied. Tetrodotoxin (1 μM; Tocris) was dissolved in citrate buffer and 4-aminopyridine (500 μM; Tocris) was dissolved in water.

Solutions—Dissecting/slicing aCSF contained (mM) 250 sucrose, 3 KCl, 2 $MgSO_4$, 1.2 NaH_2PO_4, 10 D-glucose, 25 $NaHCO_3$, 0.1 $CaCl_2$. Recording aCSF contained (mM) 126 NaCl, 2.5 KCl, 1.2 NaH_2PO_4, 1.2 $MgCl_2$ 11 D-glucose, 18 $NaHCO_3$, 2 $CaCl_2$[97]. Internal solution contained (mM) 130 K-gluconate, 20 HEPES, 2 NaCl, 4 $MgCl_2$, 0.25 EGTA, 4 Na-ATP, 0.4 Na-GTP[98] and 0.25 % biocytin, and was adjusted to pH 7.2. At all stages, aCSF was equilibrated with carbogen (95% O_2; 5% CO_2). A liquid junction potential of 14 mV was corrected offline.

Behavioral Testing

Littermate controls were used for behavioral tests, and the experimenter was blinded to genotype/treatment. Animals were habituated to the behavioral testing apparatus for 1 h on each of the two days preceding data collection, and for 30 min on the day of testing. Tests

Author Manuscript Author Manuscript Author Manuscript Author Manuscript

were conducted at 7-8 weeks, or at 12-16 weeks for mice that received intracranial surgery for viral injections or cannula/optic fiber implantation.

Spontaneous Itch—To quantify scratching induced in the absence of an experimental mechanical stimulus (spontaneous itch), mice were placed in a plastic chamber and video-recorded for a period of 30 min; bouts of hindlimb scratching were counted offline[4].

Mechanical Itch—To quantify itch-related scratching behaviors induced by mechanical stimulation of the hairy skin, mice were placed in a plastic chamber and a 0.7 g von Frey hair was applied to the nape for 1 s[4]. Mice received 10 stimulations at an interval of 1 min, and data were presented as the percentage of trials in which scratching was evoked.

Chemical itch—The pruritogens chloroquine (200 μg; Sigma), histamine (100 μg; Sigma), compound 48/80 (100 μg; Sigma), SLIGRL-NH_2 (SLIGRL; 100 μM; Abcam), 5-hydroxytryptamine (5-HT; 100 μM; Tocris); ß-alanine (50 mM; Sigma) were dissolved in 0.9% sterile saline and injected intradermally behind the ear or, for cannulated mice, the nape in a volume of 50 μl. The behavior of each animal was video recorded over the following 30 min, and the number of hindpaw scratch bouts was counted.

von Frey—Mice were placed in a plexiglass chamber on an elevated wire grid and the lateral plantar surface of the hindpaw was stimulated with calibrated von Frey monofilaments (0.008-4 g). The paw withdrawal threshold for the von Frey assay was determined by Dixon's up-down method[99].

Brush—Mice were placed in a plexiglass chamber on an elevated wire grid and the plantar surface of the hindpaw was stimulated by light stroking with a fine paintbrush in a heel-to-toe direction[91]. The test was repeated 10 times at 10 s intervals between trails, and the percentage of positive paw-withdrawal trials was calculated.

Pinprick—Mice were placed in a plastic chamber on an elevated wire grid and the plantar surface of the hindpaw was stimulated with an Austerlitz insect pin (Tip diameter: 0.02 mm; Fine Science Tools). The pin was gently applied to the plantar surface of the hindpaw without moving the paw or penetrating the skin. The pin stimulation was repeated 10 times on different paw areas with a 1-2 min interval between trails, and the percentage of trials in which mice responded with paw withdrawal was calculated.

Pinch—Mice were placed in a plexiglass chamber for 15 min, and then an alligator clip producing 340 g force was applied to the ventral skin surface between the footpad and the heel. Mice were video recorded for 60 s and licking episodes were counted.

Randall-Selitto—Prior to testing, mice were placed in a plastic restraining tube and allowed 5 min to acclimatize. A Randall-Selitto device (IITC, USA) was used to apply slowly increasing pressure to a point midway along the tail until the animal showed clear signs of discomfort. This pressure was recorded as the pain threshold. Three trials taken at 2 min intervals were performed to calculate the average threshold for each animal.

Author Manuscript Author Manuscript Author Manuscript Author Manuscript

Hot Plate—Mice were placed on a hot plate (IITC, USA) set at 56°C and the latencies to flinching and jumping were measured, as were the numbers of licking and jumping over a 30 s period. All animals were tested sequentially with a minimum of 5 min between each test.

Hargreaves—Mice were placed in a plastic chamber and the plantar hindpaw surface was exposed to a beam of radiant heat (IITC, USA). The latency to paw withdrawal was determined in one trial per hindpaw and averaged per animal, with a 10 min interval between trials. A cutoff time of 30 s was set to prevent tissue damage.

Accelerating Rotarod Test—An accelerating rotarod test was used to measure gross motor ability and coordination. Mice were trained on the rotating rod at a constant speed of 3 rpm for three 5-min periods at an interval of 20 min on each of the two days prior to testing. Mice were then tested by accelerating the rod from 0 to 40 rpm. Each animal was subjected to three trials, with an interval of 20 min between each trial. The latency to fall was averaged for all three trials.

Alloknesis and chronic itch models

Histamine alloknesis—Histamine (50 μg in 10 μl) was administered by intradermal injection into the nape 30 min prior to testing, as previously described[51]. A 0.07 g von Frey hair was then used to deliver light punctate stimuli to a randomly selected site 5-10 mm from the injection site. Mice were assessed for hindlimb scratching immediately following each stimulus. Mice received 10 stimulations at 1 min intervals, and data were presented as a percentage.

Dry skin itch model—The nape and rostral back of mice were shaved 5 days before treatment. Treatment entailed application with a sterile cotton swab of a mixture of acetone and ether (AEW) in a ratio of 1:1 to the rostral back for 15 s, followed by distilled water for 25 s[49,50]. AEW treatment was repeated twice daily on days 1-7. On day 8, mechanical itch sensitization was assessed. Mice were first habituated for 15 min in a plexiglass chamber, and then a 0.07g von Frey filament was used to deliver 10 innocuous mechanical stimuli (~1-s duration) at an interval of 1 min to a randomly selected site on the nape at the margin of the AEW-treated area. The response rate of hindlimb scratching toward the stimulation site was quantified as a percentage. Mice continued to receive AEW treatment twice daily from day 8 to day 10. On day 10, spontaneous itch was measured as described above.

Allergic Contact Dermatitis model—The nape, rostral back and abdominal skin of mice were shaved 5 days before treatment. A micropipette was used to apply 25 μl 1% squaric acid dibutylester (SADBE) in acetone to the abdominal skin once daily on days 1-3. On days 8-10, 25 μl 1% SADBE in acetone was applied to the rostral back[2,48]. On day 11, mechanical itch sensitization was assessed as described for the dry skin itch model. On day 12, spontaneous itch was assessed as described above.

Quantification and Statistical Analysis

Data were analyzed in GraphPad Prism 9.2 (Graphpad Software) or Excel 16 (Microsoft) by two-way ANOVA with Šidák post hoc correction, or by two-tailed t-tests. $p < 0.05$ was

Author Manuscript Author Manuscript Author Manuscript Author Manuscript

considered to be statistically significant. All data are presented as the mean ± standard error of the mean (SEM).

Supplementary Material

Refer to Web version on PubMed Central for supplementary material.

ACKNOWLEDGMENTS

This study was supported by NIH grant NS111643 to M.G., NIH grant 5R01MH116203 to S.H. and a Salk Innovation Grant to M.G. and S.H. Viruses were supplied by the Salk Institute Viral Core Facility. M.G. holds the Frederick W. and Joanna. J. Mitchell Chair.

REFERENCES

1. Sanders KZ, Fast K, and Yosipovitch G (2019). Why we scratch: Function and dysfunction. Exp. Dermatol 28, 1482–1484. 10.1111/exd.13977. [PubMed: 31132174]
2. Pan H, Fatima M, Li A, Lee H, Cai W, Horwitz L, Hor CC, Zaher N, Cin M, Slade H, et al. (2019). Identification of a Spinal Circuit for Mechanical and Persistent Spontaneous Itch. Neuron 103, 1135–1149.e6. 10.1016/j.neuron.2019.06.016. [PubMed: 31324538]
3. Acton D, Ren X, Di Costanzo S, Dalet A, Bourane S, Bertocchi I, Eva C, and Goulding M (2019). Spinal Neuropeptide Y1 Receptor-Expressing Neurons Form an Essential Excitatory Pathway for Mechanical Itch. Cell Rep. 28, 625–639.e6. 10.1016/j.celrep.2019.06.033. [PubMed: 31315043]
4. Bourane S, Duan B, Koch SC, Dalet A, Britz O, Garcia-Campmany L, Kim E, Cheng L, Ghosh A, Ma Q, et al. (2015). Gate control of mechanical itch by a subpopulation of spinal cord interneurons. Science (80-.). 350, 550–554. 10.1126/science.aac8653.
5. Sun YG, and Chen ZF (2007). A gastrin-releasing peptide receptor mediates the itch sensation in the spinal cord. Nature 448, 700–703. 10.1038/nature06029. [PubMed: 17653196]
6. Sun YG, Zhao ZQ, Meng XL, Yin J, Liu XY, and Chen ZF (2009). Cellular basis of itch sensation. Science (80-.). 325, 1531–1534. 10.1126/science.1174868.
7. Ross SE, Mardinly AR, McCord AE, Zurawski J, Cohen S, Jung C, Hu L, Mok SI, Shah A, Savner EM, et al. (2010). Loss of Inhibitory Interneurons in the Dorsal Spinal Cord and Elevated Itch in Bhlhb5 Mutant Mice. Neuron 65, 886–898. 10.1016/j.neuron.2010.02.025. [PubMed: 20346763]
8. Hall M (1833). On the reflex function of the medulla oblongata and medulla spi-nalis. Philos. Trans. R. Soc. London 123, 635–665. 10.1098/rstl.1833.0028.
9. Sherrington CS (1906). Observations on the scratch-reflex in the spinal dog. J. Physiol 34, 1. 10.1113/jphysiol.1906.sp001139. [PubMed: 16992835]
10. Sherrington CS, and Laslett EE (1903). Observations on some spinal reflexes and the interconnection of spinal segments. J. Physiol 29, 58–96. 10.1113/jphysiol.1903.sp000946. [PubMed: 16992657]
11. Mu D, Deng J, Liu K-F, Wu Z-Y, Shi Y-F, Guo W-M, Mao Q-Q, Liu X-J, Li H, and Sun Y-G (2017). A central neural circuit for itch sensation. Science (80-.). 357, 695–699. 10.1126/science.aaf4918.
12. Campos CA, Bowen AJ, Roman CW, and Palmiter RD (2018). Encoding of danger by parabrachial CGRP neurons. Nature 555, 617–622. 10.1038/nature25511. [PubMed: 29562230]
13. Ikoma A, Steinhoff M, Ständer S, Yosipovitch G, and Schmelz M (2006). The neurobiology of itch. Nat. Rev. Neurosci 7, 535–547. 10.1038/nrn1950. [PubMed: 16791143]
14. Papoiu ADP, Coghill RC, Kraft RA, Wang H, and Yosipovitch G (2012). A tale of two itches. Common features and notable differences in brain activation evoked by cowhage and histamine induced itch. Neuroimage 59, 3611–3623. 10.1016/j.neuroimage.2011.10.099. [PubMed: 22100770]

Author Manuscript Author Manuscript Author Manuscript Author Manuscript

15. Vierow V, Forster C, Vogelgsang R, Dörfler A, and Handwerker HO (2015). Cerebral networks linked to itch-related sensations induced by histamine and capsaicin. Acta Derm. Venereol 95, 645–652. 10.2340/00015555-2006. [PubMed: 25387448]
16. Hsieh JC, Hagermark O, Stahle-Backdahl M, Ericson K, Eriksson L, Stone-Elander S and Ingvar M (1994). Urge to scratch represented in the human cerebral cortex during itch. J. Neurophysiol 72, 3004–3008. 10.1152/jn.1994.72.6.3004. [PubMed: 7897505]
17. Darsow U, Drzezga A, Frisch M, Munz F, Weilke F, Bartenstein P, Schwaiger M, and Ring J (2000). Processing of histamine-induced itch in the human cerebral cortex: A correlation analysis with dermal reactions. J. Invest. Dermatol 115, 1029–1033. 10.1046/j.1523-1747.2000.00193.x. [PubMed: 11121137]
18. Sanders KM, Sakai K, Henry TD, Hashimoto T, and Akiyama T (2019). A subpopulation of amygdala neurons mediates the affective component of itch. J. Neurosci 39, 3345–3356. 10.1523/jneurosci.2759-18.2019. [PubMed: 30819800]
19. Samineni VK, Grajales-Reyes JG, Grajales-Reyes GE, Tycksen E, Copits BA, Pedersen C, Ankudey ES, Sackey JN, Sewell SB, Bruchas MR, et al. (2021). Cellular, circuit and transcriptional framework for modulation of itch in the central Amygdala. Elife 10. 10.7554/elife.68130.
20. Mu D, and Sun YG (2017). Itch induces conditioned place aversion in mice. Neurosci. Lett 658, 91–96. 10.1016/j.neulet.2017.08.046. [PubMed: 28842279]
21. Abraira VE, and Ginty DD (2013). The Sensory Neurons of Touch. Neuron 79, 618–639. 10.1016/j.neuron.2013.07.051. [PubMed: 23972592]
22. Petit D, and Burgess PR (1968). Dorsal column projection of receptors in cat hairy skin supplied by myelinated fibers. J. Neurophysiol 31, 849–855. 10.1152/jn.1968.31.6.849. [PubMed: 5710538]
23. Gauriau C, and Bernard JF (2002). Pain pathways and parabrachial circuits in the rat. Exp. Physiol 87, 251–258. 10.1113/eph8702357. [PubMed: 11856971]
24. Todd AJ (2010). Neuronal circuitry for pain processing in the dorsal horn. Nat. Rev. Neurosci 11, 823–836. 10.1038/nrn2947. [PubMed: 21068766]
25. Britz O, Zhang J, Grossmann KS, Dyck J, Kim JC, Dymecki S, Gosgnach S, and Goulding M (2015). A genetically defined asymmetry underlies the inhibitory control of flexor-extensor locomotor movements. Elife 4, e04718. 10.7554/elife.04718. [PubMed: 26465208]
26. Han S, Soleiman M, Soden M, Zweifel L, and Palmiter RD (2015). Elucidating an Affective Pain Circuit that Creates a Threat Memory. Cell 162, 363–374. 10.1016/j.cell.2015.05.057. [PubMed: 26186190]
27. Bernard J-F, Dallel R, Raboisson P, Villanueva L, and Bars D. Le (1995). Organization of the efferent projections from the spinal cervical enlargement to the parabrachial area and periaqueductal graye. A PHA-L study in the rat. J. Comp. Neurol 353, 480–505. 10.1002/cne.903530403. [PubMed: 7759612]
28. Al-Khater KM, and Todd AJ (2009). Collateral projections of neurons in laminae I, III, and IV of rat spinal cord to thalamus, periaqueductal gray matter, and lateral parabrachial area. J. Comp. Neurol 515, 629–646. 10.1002/cne.22081. [PubMed: 19496168]
29. Choi S, Hachisuka J, Brett MA, Magee AR, Omori Y, Iqbal N. ul A., Zhang D, DeLisle MM, Wolfson RL, Bai L, et al. (2020). Parallel ascending spinal pathways for affective touch and pain. Nature 587, 258–263. 10.1038/s41586-020-2860-1. [PubMed: 33116307]
30. Usoskin D, Furlan A, Islam S, Abdo H, Lönnerberg P, Lou D, Hjerling-Leffler J, Haeggström J, Kharchenko O, Kharchenko P, et al. (2015). Unbiased classification of sensory neuron types by large-scale single-cell RNA sequencing. Nat. Neurosci 18, 145–153. 10.1038/nn.3881. [PubMed: 25420068]
31. Dong X, and Dong X (2018). Peripheral and Central Mechanisms of Itch. Neuron 98, 482–494. 10.1016/j.neuron.2018.03.023. [PubMed: 29723501]
32. Shimada SG, and LaMotte RH (2008). Behavioral differentiation between itch and pain in mouse. Pain 139, 681–687. 10.1016/j.pain.2008.08.002. [PubMed: 18789837]
33. Liu T, Han Q, Chen G, Huang Y, Zhao LX, Berta T, Gao YJ, and Ji RR (2016). Toll-like receptor 4 contributes to chronic itch, alloknesis, and spinal astrocyte activation in male mice. Pain 157, 806–817. 10.1097/j.pain.0000000000000439. [PubMed: 26645545]

Author Manuscript Author Manuscript Author Manuscript Author Manuscript

34. Chung K, Pitcher T, Grant AD, Hewitt E, Lindstrom E, and Malcangio M (2019). Cathepsin S acts via protease-activated receptor 2 to activate sensory neurons and induce itch-like behaviour. Neurobiol. Pain 6. 10.1016/j.ynpai.2019.100032.
35. Morita T, McClain SP, Batia LM, Pellegrino M, Wilson SR, Kienzler MA, Lyman K, Olsen ASB, Wong JF, Stucky CL, et al. (2015). HTR7 Mediates Serotonergic Acute and Chronic Itch. Neuron 87, 124–138. 10.1016/j.neuron.2015.05.044. [PubMed: 26074006]
36. Akiyama T, Carstens MI, and Carstens E (2010). Facial Injections of Pruritogens and Algogens Excite Partly Overlapping Populations of Primary and Second-Order Trigeminal Neurons in Mice. J. Neurophysiol 104, 2442. 10.1152/jn.00563.2010. [PubMed: 20739601]
37. Liu Q, Sikand P, Ma C, Tang Z, Han L, Li Z, Sun S, LaMotte RH, and Dong X (2012). Mechanisms of itch evoked by β-alanine. J. Neurosci 32, 14532–14537. 10.1523/jneurosci.3509-12.2012. [PubMed: 23077038]
38. Gray PA (2008). Transcription factors and the genetic organization of brain stem respiratory neurons. J. Appl. Physiol 104, 1513–1521. 10.1152/japplphysiol.01383.2007. [PubMed: 18218908]
39. Miller RL, Knuepfer MM, Wang MH, Denny GO, Gray PA, and Loewy AD (2012). Fos-activation of FoxP2 and Lmx1b neurons in the parabrachial nucleus evoked by hypotension and hypertension in conscious rats. Neuroscience 218, 110–125. 10.1016/j.neuroscience.2012.05.049. [PubMed: 22641087]
40. Stein MK, and Loewy AD (2010). Area postrema projects to FoxP2 neurons of the pre-locus coeruleus and parabrachial nuclei: Brainstem sites implicated in sodium appetite regulation. Brain Res. 1359, 116–127. 10.1016/j.brainres.2010.08.085. [PubMed: 20816675]
41. Karthik S, Huang D, Delgado Y, Laing JJ, Peltekian L, Iverson GN, Grady F, Miller RL, McCann CM, Fritzsch B, et al. (2022). Molecular ontology of the parabrachial nucleus. J. Comp. Neurol 530, 1658–1699. 10.1002/cne.25307. [PubMed: 35134251]
42. Doyle MW, and Andresen MC (2001). Reliability of monosynaptic sensory transmission in brain stem neurons in vitro. J. Neurophysiol 85, 2213–2223. [PubMed: 11353036]
43. Sugimura YK, Takahashi Y, Watabe AM, and Kato F (2016). Synaptic and network consequences of monosynaptic nociceptive inputs of parabrachial nucleus origin in the central amygdala. J. Neurophysiol 115, 2721–2739. 10.1152/jn.00946.2015. [PubMed: 26888105]
44. Gao ZR, Chen WZ, Liu MZ, Chen XJ, Wan L, Zhang XY, Yuan L, Lin JK, Wang M, Zhou L, et al. (2019). Tac1-Expressing Neurons in the Periaqueductal Gray Facilitate the Itch-Scratching Cycle via Descending Regulation. Neuron 101, 45–59.e9. 10.1016/j.neuron.2018.11.010. [PubMed: 30554781]
45. Samineni VK, Grajales-Reyes JG, Sundaram SS, Yoo JJ, and Gereau RW (2019). Cell type-specific modulation of sensory and affective components of itch in the periaqueductal gray. Nat. Commun 2019 101 10, 1–15. 10.1038/s41467-019-12316-0.
46. Wu ZH, Shao HY, Fu YY, Wu XB, Cao DL, Yan SX, Sha WL, Gao YJ, and Zhang ZJ (2021). Descending Modulation of Spinal Itch Transmission by Primary Somatosensory Cortex. Neurosci. Bull 37, 1345–1350. 10.1007/s12264-021-00713-9. [PubMed: 34057697]
47. Wahlgren CF (1999). Itch and atopic dermatitis: An overview. J. Dermatol 26, 770–779. 10.1111/j.1346-8138.1999.tb02090.x. [PubMed: 10635621]
48. Scott AE, Kashon ML, Yucesoy B, Luster MI, and Tinkle SS (2002). Insights into the Quantitative Relationship between Sensitization and Challenge for Allergic Contact Dermatitis Reactions. Toxicol. Appl. Pharmacol 183, 66–70. 10.1006/taap.2002.9469. [PubMed: 12217643]
49. Miyamoto T, Nojima H, Shinkado T, Nakahashi T, and Kuraishi Y (2002). Itch-associated response induced by experimental dry skin in mice. Jpn. J. Pharmacol 88, 285–292. 10.1254/jjp.88.285. [PubMed: 11949883]
50. Nojima H, Carstens MI, and Carstens E (2003). C-Fos Expression in Superficial Dorsal Horn of Cervical Spinal Cord Associated With Spontaneous Scratching in Rats With Dry Skin. Neurosci. Lett 347, 62–64. 10.1016/s0304-3940(03)00609-8. [PubMed: 12865142]
51. Akiyama T, Carstens MI, Ikoma A, Cevikbas F, Steinhoff M, and Carstens E (2012). Mouse model of touch-evoked itch (alloknesis). J. Invest. Dermatol 132, 1886–1891. 10.1038/jid.2012.52. [PubMed: 22418875]

Author Manuscript Author Manuscript Author Manuscript Author Manuscript

52. Goulding M, Lanuza G, Sapir T, and Narayan S (2002). The formation of sensorimotor circuits. Curr. Opin. Neurobiol 12, 508–515. 10.1016/S0959-4388(02)00371-9. [PubMed: 12367629]

53. Lai HC, Seal RP, and Johnson JE (2016). Making sense out of spinal cord somatosensory development. Development 143, 3434–3448. 10.1242/dev.139592. [PubMed: 27702783]

54. Akiyama T, Nguyen T, Curtis E, Nishida K, Devireddy J, Delahanty J, Carstens MI, and Carstens E (2015). A central role for spinal dorsal horn neurons that express neurokinin-1 receptors in chronic itch. Pain 156, 1240–1246. 10.1097/j.pain.0000000000000172. [PubMed: 25830923]

55. Sheahan TD, Warwick CA, Fanien LG, and Ross SE (2020). The Neurokinin-1 Receptor is Expressed with Gastrin-Releasing Peptide Receptor in Spinal Interneurons and Modulates Itch. J. Neurosci 40, 8816–8830. 10.1523/jneurosci.1832-20.2020. [PubMed: 33051347]

56. Davidson S, Zhang X, Yoon CH, Khasabov SG, Simone DA, Giesler GJ Jr, and (2007). The itch-producing agents histamine and cowhage activate separate populations of primate spinothalamic tract neurons. J. Neurosci 27, 10007–10014. 10.1523/jneurosci.2862-07.2007. [PubMed: 17855615]

57. Davidson S, Zhang X, Khasabov SG, Moser HR, Honda CN, Simone DA, and Giesler GJ (2012). Pruriceptive spinothalamic tract neurons: physiological properties and projection targets in the primate. J. Neurophysiol 108, 1711–1723. 10.1152/jn.00206.2012. [PubMed: 22723676]

58. Davidson S, and Giesler GJ (2010). The multiple pathways for itch and their interactions with pain. Trends Neurosci. 33, 550–558. 10.1016/j.tins.2010.09.002. [PubMed: 21056479]

59. Li JN, Ren JH, Zhao LJ, Wu XM, Li H, Dong YL, and Li YQ (2021). Projecting neurons in spinal dorsal horn send collateral projections to dorsal midline/intralaminar thalamic complex and parabrachial nucleus. Brain Res. Bull 169, 184–195. 10.1016/j.brainresbull.2021.01.012. [PubMed: 33508400]

60. Huang T, Lin SH, Malewicz NM, Zhang Y, Zhang Y, Goulding M, LaMotte RH, and Ma Q (2019). Identifying the pathways required for coping behaviours associated with sustained pain. Nature 565, 86–90. 10.1038/s41586-018-0793-8. [PubMed: 30532001]

61. Saper CB (1982). Reciprocal parabrachial-cortical connections in the rat. Brain Res. 242, 33–40. 10.1016/0006-8993(82)90493-0. [PubMed: 7104731]

62. Palmiter RD (2018). The Parabrachial Nucleus: CGRP Neurons Function as a General Alarm. Trends Neurosci. 41, 280–293. 10.1016/j.tins.2018.03.007. [PubMed: 29703377]

63. Barik A, Sathyamurthy A, Thompson J, Seltzer M, Levine A, and Chesler A (2021). A spinoparabrachial circuit defined by Tacr1 expression drives pain. Elife 10, 1–42. 10.7554/elife.61135.

64. Kardon AP, Polgár E, Hachisuka J, Snyder LM, Cameron D, Savage S, Cai X, Karnup S, Fan CR, Hemenway GM, et al. (2014). Dynorphin Acts as a Neuromodulator to Inhibit Itch in the Dorsal Horn of the Spinal Cord. Neuron 82, 573–586. 10.1016/j.neuron.2014.02.046. [PubMed: 24726382]

65. Bickford R (1938). Experiments relating to the itch sensation, its peripheral mechanism, and central pathways. Clin. Sci 3, 377–386.

66. Hyndman OR, and Wolkin J (1943). Anterior Chordotomy: Further Observations on Physiologic Results and Optimum Manner of Performance. Arch. Neurol. Psychiatry 50, 129–148. 10.1001/archneurpsyc.1943.02290200029002.

67. Haycraft JB (1890). Reflex Spinal Scratching Movements in Some Vertebrates. Brain 12, 516–519. 10.1093/brain/12.4.516.

68. Brown TG (1909). Studies in the Reflexes of the Guinea-Pig. I. The Scratch-Reflex in Relation to “Brown-Séquard’s Epilepsy.” Q. J. Exp. Physiol 2, 243–275. 10.1113/expphysiol.1909.sp000039.

69. Sherrington CS (1910). Notes on the Scratch-Reflex of the Cat. Q. J. Exp. Physiol 3, 213–220. 10.1113/expphysiol.1910.sp000065.

70. Agostinelli LJ, and Bassuk AG (2021). Novel inhibitory brainstem neurons with selective projections to spinal lamina I reduce both pain and itch. J. Comp. Neurol 529, 2125–2137. 10.1002/cne.25076. [PubMed: 33247430]

71. Deng J, Zhou H, Lin JK, Shen ZX, Chen WZ, Wang LH, Li Q, Mu D, Wei YC, Xu XH, et al. (2020). The Parabrachial Nucleus Directly Channels Spinal Nociceptive Signals to

Author Manuscript Author Manuscript Author Manuscript Author Manuscript

the Intralaminar Thalamic Nuclei, but Not the Amygdala. Neuron 107, 909–923.e6. 10.1016/j.neuron.2020.06.017. [PubMed: 32649865]

72. Follansbee T, Domocos D, Nguyen E, Nguyen A, Bountouvas A, Velasquez L, Carstens MI, Takanami K, Ross SE, and Carstens E (2022). Inhibition of itch by neurokinin 1 receptor (Tacr1)-expressing ON cells in the rostral ventromedial medulla in mice. Elife 11. 10.7554/elife.69626.
73. Huang D, Grady FS, Peltekian L, and Geerling JC (2021). Efferent projections of Vglut2, Foxp2, and Pdyn parabrachial neurons in mice. J. Comp. Neurol 529, 657–693. 10.1002/cne.24975. [PubMed: 32621762]
74. Huang D, Grady FS, Peltekian L, Laing JJ, and Geerling JC (2021). Efferent projections of CGRP/Calca-expressing parabrachial neurons in mice. J. Comp. Neurol 529, 2911–2957. 10.1002/cne.25136. [PubMed: 33715169]
75. Mu D, and Sun Y-G (2021). Circuit Mechanisms of Itch in the Brain. J. Invest. Dermatol 10.1016/j.jid.2021.09.022.
76. Zhao ZQ, Liu XY, Jeffry J, Karunarathne WKA, Li JL, Munanairi A, Zhou XY, Li H, Sun YG, Wan L, et al. (2014). Descending control of itch transmission by the serotonergic system via 5-HT1A-facilitated GRP-GRPR signaling. Neuron 84, 821–834. 10.1016/j.neuron.2014.10.003. [PubMed: 25453842]
77. Chen S, Gao X-F, Zhou Y, Liu B-L, Liu X-Y, Zhang Y, Barry DM, Liu K, Jiao Y, Bardoni R, et al. (2020). A spinal neural circuitry for converting touch to itch sensation. Nat. Commun 2020 111 11, 1–14. 10.1038/s41467-020-18895-7.
78. Craig AD (2003). Pain mechanisms: Labeled lines versus convergence in central processing. Annu. Rev. Neurosci 26, 1–30. 10.1146/annurev.neuro.26.041002.131022. [PubMed: 12651967]
79. Perl ER (2007). Ideas about pain, a historical view. Nat. Rev. Neurosci 8, 71–80. 10.1038/nrn2042. [PubMed: 17180164]
80. Hachisuka J, Baumbauer KM, Omori Y, Snyder LM, Koerber HR, and Ross SE (2016). Semi-intact ex vivo approach to investigate spinal somatosensory circuits. Elite 5, 1–19. 10.7554/elife.22866.
81. Nguyen E, Lim G, Ding H, Hachisuka J, Ko MC, and Ross SE (2021). Morphine acts on spinal dynorphin neurons to cause itch through disinhibition. Sci. Transl. Med 13. 10.1126/scitranslmed.abc3774.
82. Nattkemper LA, Tey HL, Valdes-Rodriguez R, Lee H, Mollanazar NK, Albornoz C, Sanders KM, and Yosipovitch G (2018). The Genetics of Chronic Itch: Gene Expression in the Skin of Patients with Atopic Dermatitis and Psoriasis with Severe Itch. J. Invest. Dermatol 138, 1311–1317. 10.1016/j.jid.2017.12.029. [PubMed: 29317264]
83. Pereira PJS, Machado GDB, Danesi GM, Canevese FF, Reddy VB, Pereira TCB, Bogo MR, Cheng Y-C, Laedermann C, Talbot S, et al. (2015). GRPR/PI3Kγ: Partners in Central Transmission of Itch. J. Neurosci 35, 16272–16281. 10.1523/jneurosci.2310-15.2015. [PubMed: 26658875]
84. Rousso DL, Qiao M, Kagan RD, Yamagata M, Palmiter RD, and Sanes JR (2016). Two Pairs of ON and OFF Retinal Ganglion Cells Are Defined by Intersectional Patterns of Transcription Factor Expression. Cell Rep. 75, 1930–1944. 10.1016/j.celrep.2016.04.069.
85. Madisen L, Zwingman TA, Sunkin SM, Oh SW, Zariwala HA, Gu H, Ng LL, Palmiter RD, Hawrylycz MJ, Jones AR, et al. (2010). A robust and high-throughput Cre reporting and characterization system for the whole mouse brain. Nat. Neurosci 13, 133–140. 10.1038/nn.2467. [PubMed: 20023653]
86. Madisen L, Garner AR, Shimaoka D, Chuong AS, Klapoetke NC, Li L, van der Bourg A, Niino Y, Egolf L, Monetti C, et al. (2015). Transgenic mice for intersectional targeting of neural sensors and effectors with high specificity and performance. Neuron 85, 942–958. 10.1016/j.neuron.2015.02.022. [PubMed: 25741722]
87. Niederkofler V, Asher TE, Okaty BW, Rood BD, Narayan A, Hwa LS, Beck SG, Miczek KA, and Dymecki SM (2016). Identification of Serotonergic Neuronal Modules that Affect Aggressive Behavior. Cell Rep. 17, 1934–1949. 10.1016/j.celrep.2016.10.063. [PubMed: 27851959]
88. Sciolino NR, Plummer NW, Chen Y-W, Alexander GM, Robertson SD, Dudek SM, McElligott ZA, and Jensen P (2016). Recombinase-Dependent Mouse Lines for Chemogenetic Activation of Genetically Defined Cell Types. Cell Rep. 75, 2563–2573. 10.1016/j.celrep.2016.05.034.

Author Manuscript Author Manuscript Author Manuscript Author Manuscript

89. Hooks BM, Lin JY, Guo C, and Svoboda K (2015). Dual-Channel Circuit Mapping Reveals Sensorimotor Convergence in the Primary Motor Cortex. J. Neurosci 35, 4418–4426. 10.1523/jneurosci.3741-14.2015. [PubMed: 25762684]

90. Jensen EC (2013). Quantitative Analysis of Histological Staining and Fluorescence Using ImageJ. Anat. Rec 296, 378–381. 10.1002/ar.22641.

91. Bourane S, Grossmann KS, Britz O, Dalet A, Del Barrio MG, Stam FJ, Garcia-Campmany L, Koch S, and Goulding M (2015). Identification of a Spinal Circuit for Light Touch and Fine Motor Control. Cell 160, 503–515. 10.1016/j.cell.2015.01.011. [PubMed: 25635458]

92. Wiley R., and Lappi D. (1999). Targeting neurokinin-1 receptor-expressing neurons with [Sar9,Met(O2)11]substance P-saporin. Neurosci. Lett 277, 1–4. 10.1016/S0304-3940(99)00846-0. [PubMed: 10643883]

93. Collins BE, Blixt O, Han S, Duong B, Li H, Nathan JK, Bovin N, and Paulson JC (2006). High-Affinity Ligand Probes of CD22 Overcome the Threshold Set by cis Ligands to Allow for Binding, Endocytosis, and Killing of B Cells . J. Immunol 177, 2994–3003. 10.4049/jimmunol.177.5.2994. [PubMed: 16920935]

94. Weyergang A, Selbo PK, and Berg K (2006). Photochemically stimulated drug delivery increases the cytotoxicity and specificity of EGF-saporin. J. Control. Release 111, 165–173. 10.1016/j.jconrel.2005.12.002. [PubMed: 16466823]

95. Sakurada T, Manome Y, Katsumata K, Tan-No K, Sakurada S, Ohba M, and Kisara K (1994). Comparison of antagonistic effects of sendide and CP-96,345 on a spinally mediated behavioural response in mice. Eur. J. Pharmacol 261, 85–90. 10.1016/0014-2999(94)90304-2. [PubMed: 7528145]

96. Bonin RP, and De Koninck Y (2014). A spinal analog of memory reconsolidation enables reversal of hyperalgesia. Nat. Neurosci 77, 1043–1045. 10.1038/nn.3758.

97. Carter ME, Soden ME, Zweifel LS, and Palmiter RD (2013). Genetic identification of a neural circuit that suppresses appetite. Nature 503, 111. 10.1038/nature12596. [PubMed: 24121436]

98. Liu S, Ye M, Pao GM, Song SM, Jhang J, and Han S (2020). Identification of a novel breathing circuit that controls pain and anxiety. bioRxiv, 2020.01.09.900738. 10.1101/2020.01.09.900738.

99. Chaplan SR, Bach FW, Pogrel JW, Chung JM, and Yaksh TL (1994). Quantitative assessment of tactile allodynia in the rat paw. J. Neurosci. Methods 53, 55–63. [PubMed: 7990513]

Author Manuscript Author Manuscript Author Manuscript Author Manuscript

HIGHLIGHTS

- *Calcrl*$^{+}$/*Lbx1*$^{+}$ projection neurons transmit mechanical-itch from the spinal cord to the PBN
- Mechanical and chemical itch are transmitted along labeled lines to the PBN
- Separate populations of FoxP2^{+} neurons in the PBN relay mechanical and chemical itch
- Mechanical- and chemical-itch pathways are recruited together in pathological itch

Author Manuscript Author Manuscript Author Manuscript Author Manuscript

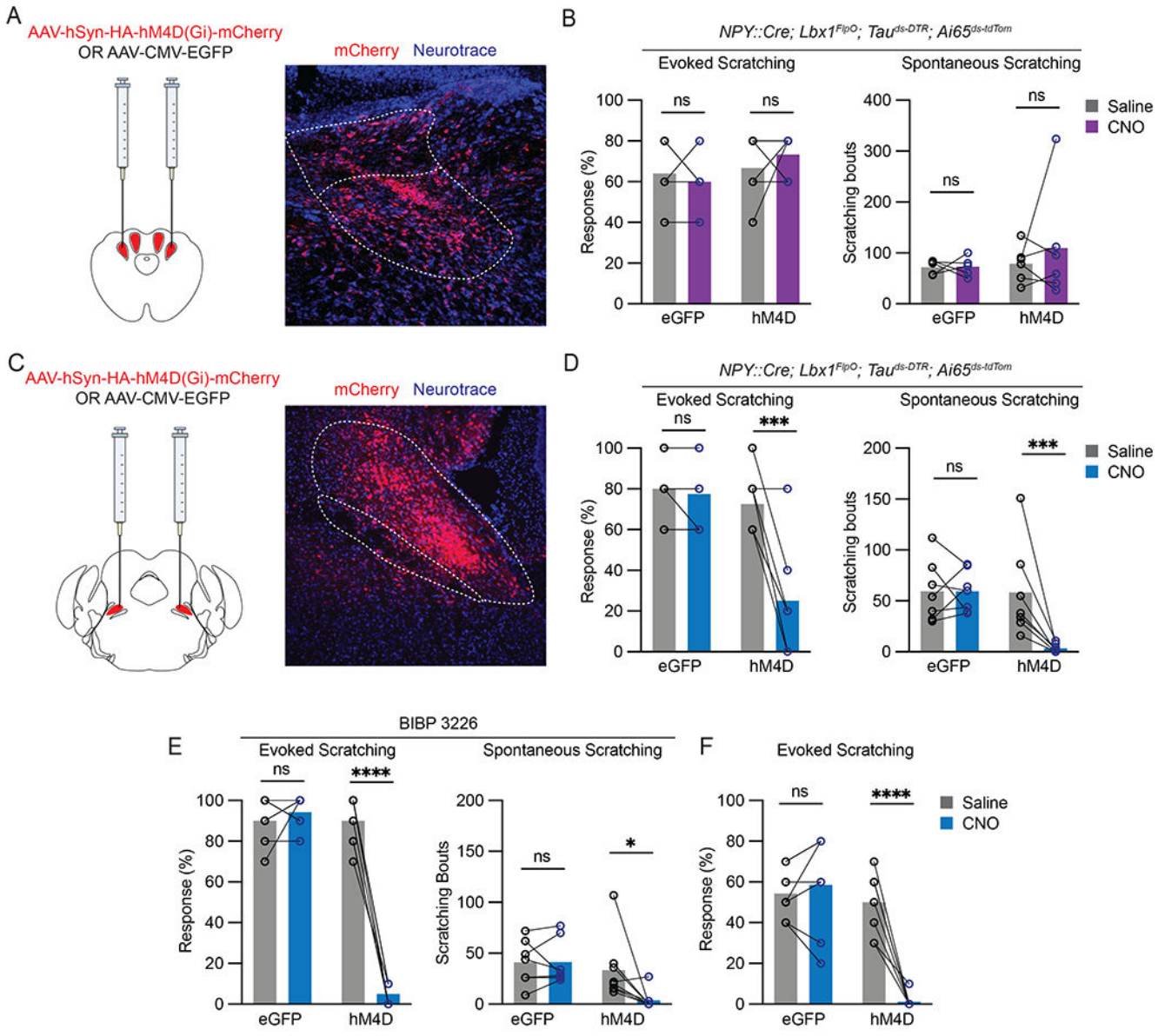

Figure 1. The PBN is essential for scratching in response to mechanical itch stimuli

(A) Strategy for viral targeting of the DCN. cu, cuneate nucleus; gr, gracile nucleus. (B) Silencing the DCN has no effect on touch-evoked (eGFP, n = 5; hM4D, n = 6) or spontaneous scratching (eGFP, n = 5; hM4D, n = 6) induced by ablation of spinal NPY^{Lbx1} neurons. (C) Strategy for viral targeting of the PBN. scp, superior cerebellar peduncle. (D) Silencing of the PBN suppresses touch-evoked (eGFP, n = 8; hM4D, n = 8) and spontaneous scratching (eGFP, n = 7; hM4D, n = 7) induced by ablation of spinal NPY^{Lbx1} neurons. (E) Silencing of the PBN reduces touch-evoked (eGFP, n = 8; hM4D, n = 8) and spontaneous scratching (eGFP, n = 7; hM4D, n = 7) following pharmacological disinhibition of the mechanical itch pathway. (F) Silencing of the PBN suppresses touch-evoked scratching (eGFP, n = 7; hM4D, n = 8) in unsensitized mice. Scale bars, 100 μm. Error bars represent SEM. Statistical differences were assessed by two-way ANOVA with Šidák post hoc

Author Manuscript Author Manuscript Author Manuscript Author Manuscript

correction. *p < 0.05; ***p < 0.001; ****p < 0.0001; ns, no significant difference. See also Figure S1.

Author Manuscript Author Manuscript Author Manuscript Author Manuscript

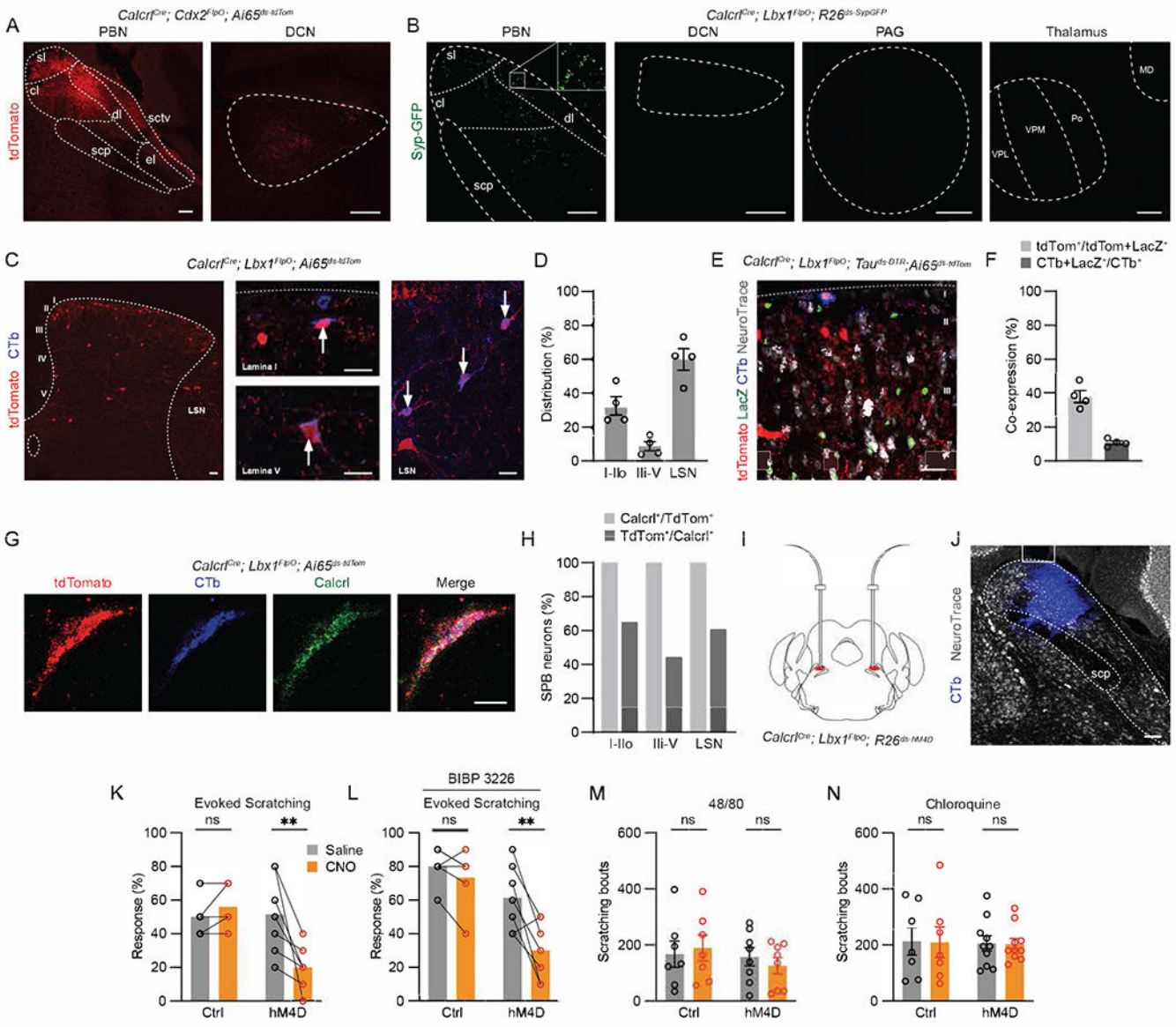

Figure 2. Calcrl^{Lbx1} SPB neurons transmit mechanical but not chemical itch

(A) Axons of spinal Calcrl^{Cdx2} neurons arborize largely in the PBN. Scale bars, 100 μm. (B) A cluster of synaptic puncta marked by synaptophysin-eGFP (Syp-GFP) derived from Calcrl^{Lbx1} projection neurons is observed in the dorsal PBN but not the DCN, PAG or thalamus. CB, cerebellum; Cl, central lateral; dl, dorsal lateral; el, external lateral; LSN, lateral spinal nucleus; MD, mediodorsal nucleus; PAG, periaqueductal gray; Po, posterior nucleus; PVT, paraventricular nucleus; scp, superior cerebellar peduncle; sctv, ventral spinocerebellar tract; sl, superior lateral; VPL, ventral posterolateral nucleus; VPM, ventral posteromedial nucleus. Scale bars, 100 μm. (C) Distribution of tdTomato$^+$ Calcrl^{Lbx1} neurons (left), and expression of tdTomato$^+$ in CTb-labeled SPB neurons in laminae I, V and the LSN. Scale bars, 20 μm. (D) Distribution of Calcrl^{Lbx1} SPB neurons (n = 4 mice). (E) tdTomato and LacZ expression in *Calcrl^{Cre}; Lbx1^{FlpO}; Tau$^{ds\text{-}DTR}$; Ai65$^{ds\text{-}tdTom}$* Scale bar, 20 μm. (F) A subset of *Caclrl^{Cre}*-expressing neurons (tdTom$^+$/LacZ$^+$) also expresses

Author Manuscript Author Manuscript Author Manuscript Author Manuscript

Lbx1^{FlpO} (tdTom^{+}). A minority of CTb-labeled SPB neurons expresses *Calcrl*^{Cre} (LacZ^{+}) but not *Lbx1*^{FlpO} (LacZ^{-}). (G) Example of a Calcrl-immunoreactive Calcrl^{Lbx1} SPB neuron. Scale bar, 10 μm. (H) All CTb-labeled Calcrl^{Lbx1} SPB neurons express Calcrl, and most Calcrl^{+} SPB neurons express tdTomato (n = 197 SPB neurons, 4 mice). (I and J) Bilateral cannula implantation into the PBN (I) and example image showing the location of cannula implantation (indicated by the box) and the spread of CTb-647 (500 nl) infused following experiments (J). Scale bar, 100 μm. (K and L) Silencing the axonal terminals of Calcrl^{Lbx1} neurons within the PBN suppresses touch-evoked itch in unsensitized mice (K; control, n = 5; hM4D, n = 7) and following disinhibition of the mechanical itch pathway (L; control, n = 6; hM4D, n = 7). (M and N) Silencing the terminals of Calcrl^{Lbx1} neurons in the PBN does not affect scratching induced by compound 48/80 (M; control, n = 7; hM4D, n = 8) or chloroquine (N; control, n = 7; hM4D, n = 10). Error bars represent SEM. Statistical differences were assessed by two-way ANOVA with Šidák post hoc correction. **$p < 0.01$; ns, no significant difference. See also Figures S2–S4.

Author Manuscript Author Manuscript Author Manuscript Author Manuscript

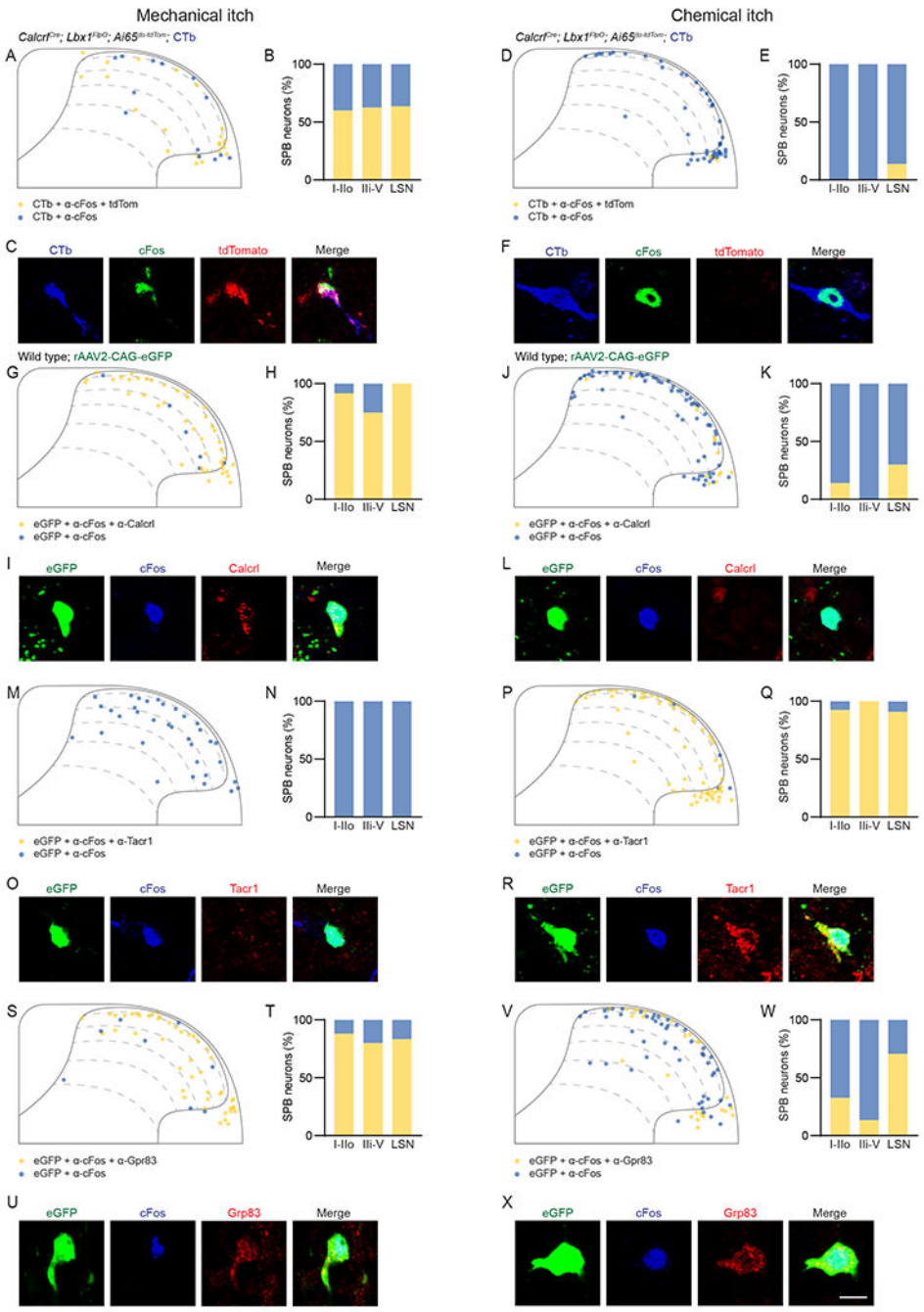

Figure 3. Distinct molecularly defined subpopulations of SPB neurons respond to mechanical and chemical itch stimuli

(A and B) A majority of CTb^{+} SPB neurons expressing cFos after mechanical itch stimulation also expresses tdTomato^{+} in *Calcrl*^{Cre};*Lbx1*^{FlpO};*Ai65*$^{ds\text{-}tdTom}$ mice. Schematic of the dorsal horn indicating the locations of tdTomato-positive and -negative mechanical itch-responsive SPB neurons (A) and summary plot (B; n = 34 CTb^{+}/cFos^{+} neurons, 4 mice). (C) Representative images of a CTb^{+}/cFos^{+}/tdTomato^{+} neuron following mechanical-itch stimulation. (D and E) Nearly all CTb^{+} SPB neurons expressing cFos after chemical-itch stimulation are tdTomato^{-} in *Calcrl*^{Cre}; *Lbx1*^{FlpO}; *Ai65*$^{ds\text{-}tdTom}$ mice (n = 49 CTb^{+}/cFos^{+}

Author Manuscript Author Manuscript Author Manuscript Author Manuscript

neurons, 4 mice). (F) Representative images of a $CTb^+/cFos^+/tdTomato^-$ neuron following chemical itch stimulation. (G and H) Nearly all $eGFP^+$ SPB neurons expressing cFos after mechanical-itch stimulation also exhibit Cacrl immunoreactivity (n = 47 $eGFP^+/cFos^+$ neurons, 4 mice). (I) Representative images of an $eGFP^+/cFos^+$ Calcrl-immunoreactive neuron. (J and K) Lack of Cacrl immunoreactivity in SPB neurons after chemical-itch stimulation (n = 68 $eGFP^+/cFos^+$ neurons, 5 mice). (L) Representative images of an $eGFP^+/cFos^+/Calcrl^-$ neuron. (M and N) No SPB neurons expressing cFos after mechanical-itch stimulation also exhibit Tacr1 immunoreactivity (n = 34 $eGFP^+/cFos^+$ neurons, 4 mice). (O) Representative images of an $eGFP^+/cFos^+/Tacr1^-$ neuron. (P and Q) Nearly all SPB neurons expressing cFos after chemical-itch stimulation exhibit Tacr1 immunoreactivity (n = 55 $eGFP^+/cFos^+$ neurons, 5 mice). (R) Representative images of an $eGFP^+/cFos^+/Tacr1^+$ neuron. (S and T) Nearly all SPB neurons expressing cFos after mechanical itch stimulation are $Gpr83^+$ (n = 52 $eGFP^+/cFos^+$ neurons, 4 mice). (U) Representative images of an $eGFP^+/cFos^+/Gpr83^+$ neuron. (V and W) Few $eGFP^+$ SPB neurons expressing cFos after chemical itch stimulation exhibit Gpr83 immunoreactivity (n = 75 $eGFP^+/cFos^+$ neurons, 5 mice). (R) Representative images of an $eGFP^+/cFos^+/Gpr83^+$ neuron. Scale bar, 10 μm. See also Figures S5, S6 and S7.

Author Manuscript Author Manuscript Author Manuscript Author Manuscript

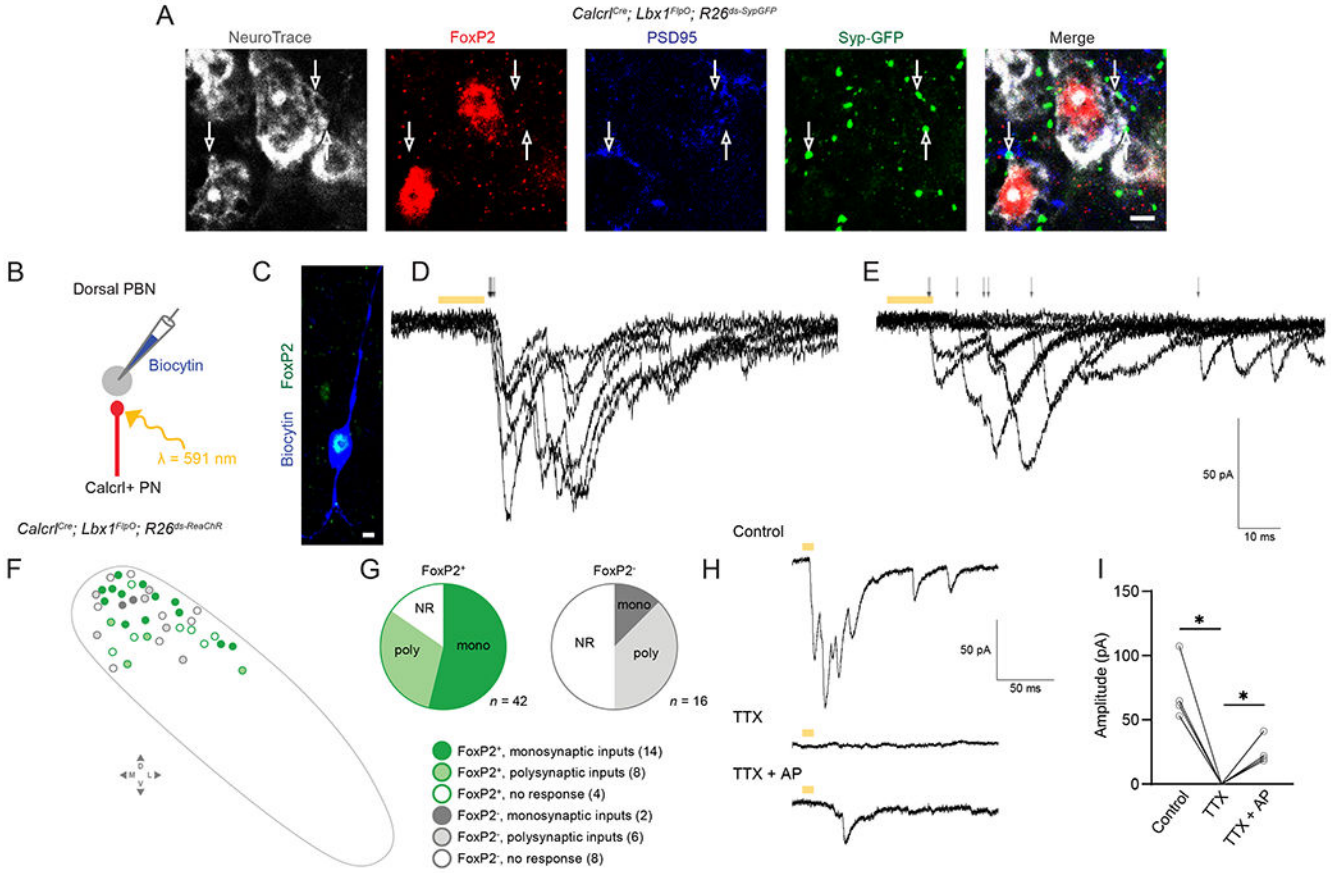

Figure 4. FoxP2^{PBN} neurons receive monosynaptic connections from spinofugal Calcrl^{Lbx1} neurons

(A) Syp-GFP^{+}/PSD95^{+} synaptic puncta derived from Calcrl^{Lbx1} SPB neurons are located in close apposition to FoxP2-immunoreactive neurons in the dorsal PBN. Scale bar, 5 μm. (B) Strategy to assess synaptic connectivity between Calcrl^{Lbx1} SPB neurons and FoxP2^{PBN} neurons in acute slices from *Calcrl^{Cre};Lbx1^{FlpO};R26$^{ds\text{-}ReaChR}$* mice. (C) A FoxP2-immunoreactive neuron infused with biocytin. Scale bar 5 μm. (D and E) Example traces showing low-jitter monosynaptic (D) and high-jitter polysynaptic EPSCs (E) evoked in FoxP2^{PBN} neurons. Arrows indicate EPSC onset times. (F and G) Diagram showing the distribution of all recorded *FoxP2*$^{+}$ and *FoxP2*$^{-}$ neurons and the type of input they receive from Calcrl^{Lbx1} neurons (F) and summary (G). (H and I) Traces from a FoxP2^{PBN} receiving monosynaptic inputs from Calcrl^{Lbx1} neurons (H) and summary plot (I; n = 4 *FoxP2*$^{+}$ neurons). In control aCSF, ReaChR stimulation of Calcrl^{Lbx1} terminals induces an EPSC, which is blocked by TTX and partially restored by AP. Statistical differences were assessed by one-way ANOVA with Šidák post hoc correction. *$p < 0.05$.

Author Manuscript Author Manuscript Author Manuscript Author Manuscript

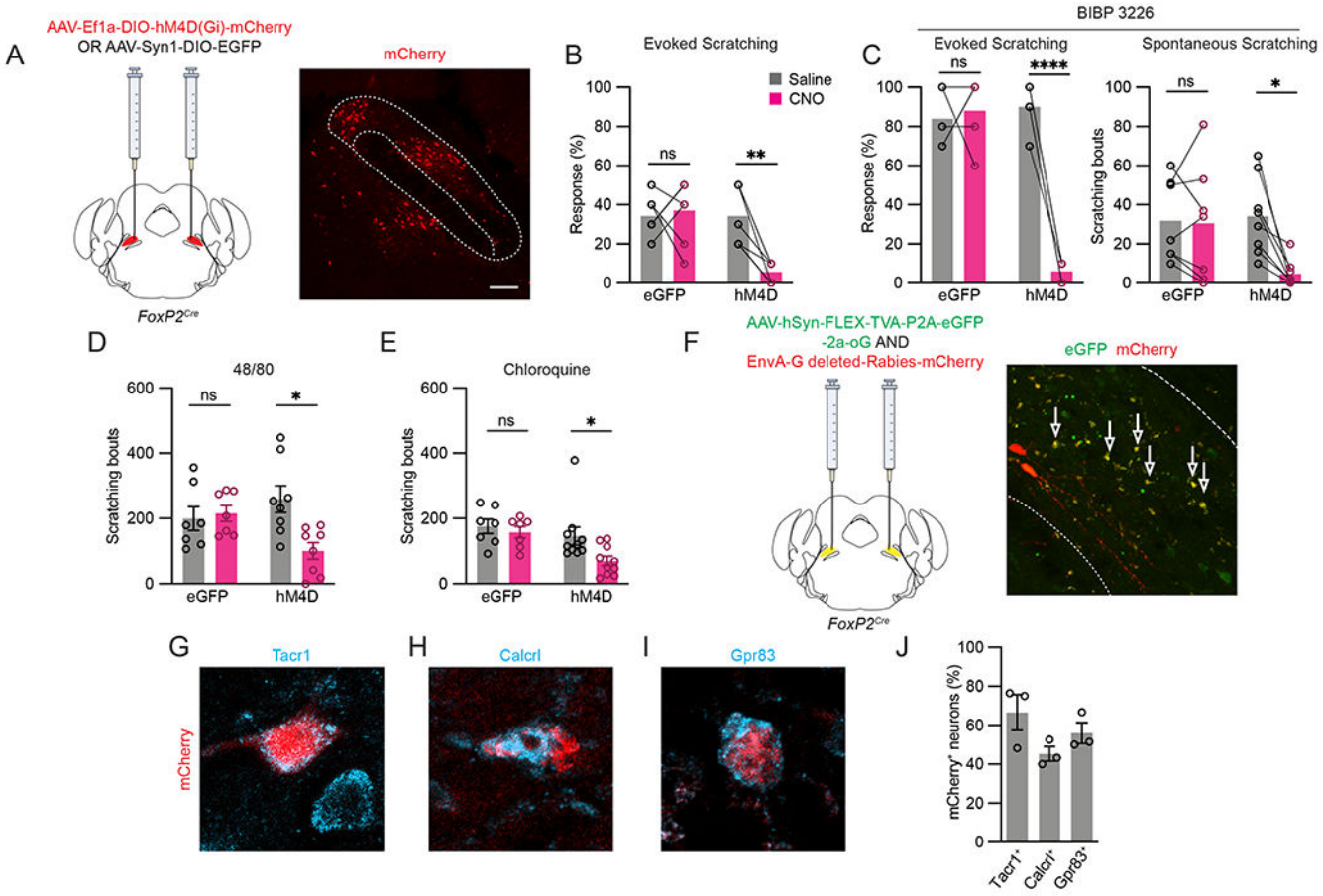

Figure 5. FoxP2^{PBN} neurons are required for protective scratching in response to mechanical or chemical itch

(A) Strategy for selectively silencing FoxP2^{PBN} neurons and an example of mCherry^{+} neurons in the lateral PBN. Scale bar, 100 μm. (B and C) Silencing FoxP2^{PBN} neurons reduces touch-evoked scratching in unsensitized mice (B; eGFP, n = 7; hM4D, n = 7) and touch-evoked (eGFP, n = 5; hM4D, n = 5) and spontaneous scratching (eGFP, n = 7; hM4D, n = 8) following disinhibition of the mechanical itch pathway (C). (D and E) Silencing FoxP2^{PBN} neurons reduces scratching induced by compound 48/80 (D; eGFP, n = 7; hM4D, n = 8) and chloroquine (E; eGFP, n = 7; hM4D, n = 10). (F) Strategy for monosynaptic retrograde tracing from FoxP2^{PBN} neurons, and an example of eGFP^{+}/mCherry^{+} starter cells in the lateral PBN. Scale bar, 25 μm. (G-J) Representative images from cervical spinal cord sections showing Tacr1 (G), Calcrl (H) and Gpr83 (I) immunoreactivity in mCherry-labeled neurons presynaptic to FoxP2^{PBN} neurons and summary (J). Scale bar, 10μm. Error bars represent SEM. Statistical differences were assessed by two-way ANOVA with Šidák post hoc correction. *p < 0.05; **p < 0.01; ****p < 0.0001; ns, no significant difference. See also Figures S8.

Author Manuscript Author Manuscript Author Manuscript Author Manuscript

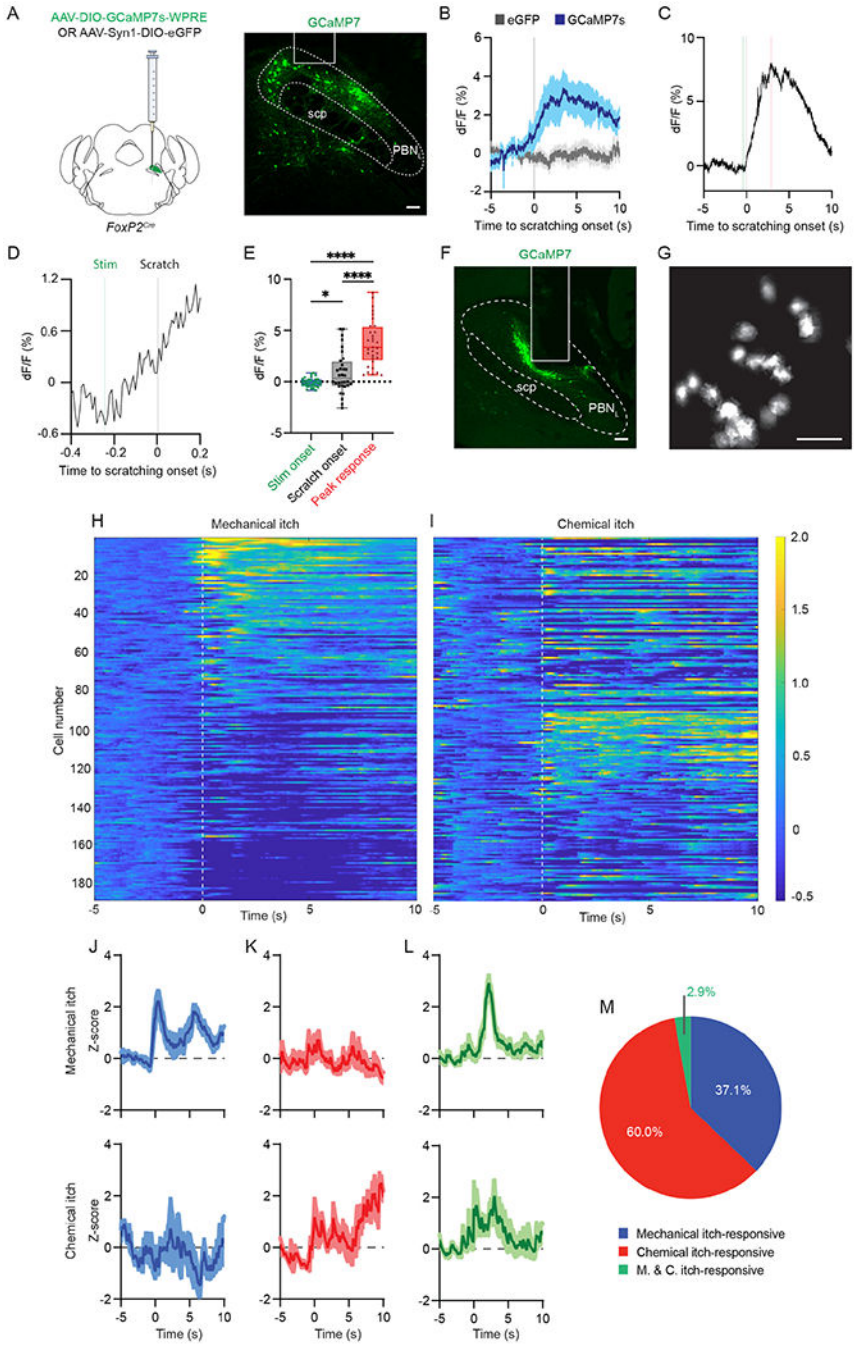

Figure 6. Discrete subpopulations of FoxP2^{PBN} neurons transmit mechanical- and chemical-itch information from the spinal cord

(A) Strategy for imaging FoxP2^{PBN} neurons by fiber photometry, and a representative image of GCaMP7s-labeled neurons in the lateral PBN. Box indicates site of optic-fiber implantation. (B) Intracellular calcium increases prior to touch-evoked scratching, indicated at 0 s (eGFP, n = 2 mice, 15 trials; GCaMP7s, n = 5 mice, 32 trials). (C and D) Representative trace (C) and expanded trace (D) showing intracellular calcium increases following mechanical-itch stimulation (green line) and prior to the onset of a scratch bout (black line), before reaching a peak (red line). (E) Summary of calcium flux values (n

Author Manuscript Author Manuscript Author Manuscript Author Manuscript

= 5 mice, 32 trials). (F) GCaMP expression and position of GRIN lens implantation in the PBN. (G) Single FoxP2^{PBN} neurons visualized under miniscope. (H and I) Calcium activities of individual FoxP2^{PBN} neurons relative to scratching, indicated at 0 s, induced by mechanical- (H) or chemical-itch (I) stimulation. (J-M) Representative calcium traces from three neurons responsive to mechanical- (J), chemical- (K), or mechanical- and chemical-itch (L) stimulation and summary (M). Solid lines indicate sample means; shaded areas indicate SEM. Scale bars, 100 μm. Statistical differences were assessed by two-way ANOVA with Šidák post hoc correction. *$p < 0.05$; ****$p < 0.0001$

Author Manuscript Author Manuscript Author Manuscript Author Manuscript

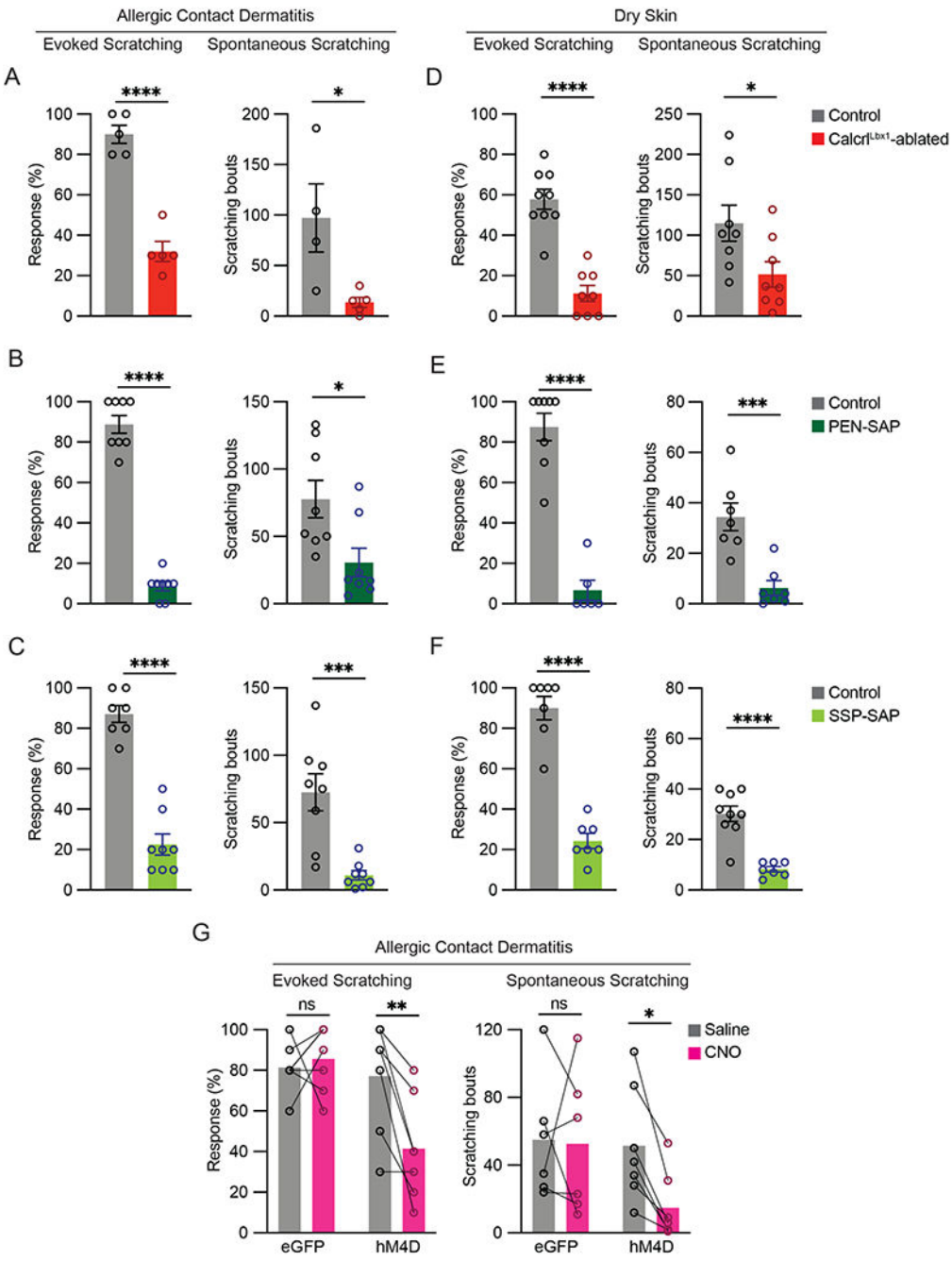

Figure 7. Separate transmission pathways for mechanical and chemical itch are both recruited in chronic itch

(A) Ablation of Calcrl^{Lbx1} neurons suppresses hyperknesis/alloknesis (control, n = 5; ablated, n = 5) and spontaneous scratching (control, n = 4; ablated, n = 5) in allergic contact dermatitis. (B) Ablation of Gpr83^{+} neurons suppresses hyperknesis/alloknesis (control, n = 9; ablated, n = 8) and spontaneous scratching (control, n = 8; ablated, n = 8) in allergic contact dermatitis. (C) Ablation of Tacr1^{+} neurons suppresses hyperknesis/alloknesis (control, n = 7; ablated, n = 8) and spontaneous scratching (control, n = 8; ablated, n = 8) in allergic contact dermatitis. (D) Ablation of Calcrl^{Lbx1} neurons suppresses

Author Manuscript Author Manuscript Author Manuscript Author Manuscript

hyperknesis/alloknesis (control, n = 9; ablated, n = 8) and spontaneous scratching (control, n = 8; ablated, n = 8) in dry skin itch. (E) Ablation of $Gpr83^{+}$ neurons suppresses hyperknesis/alloknesis (control, n = 8; ablated, n = 6) and spontaneous scratching (control, n = 7; ablated, n = 7) in dry skin itch. (F) Ablation of $Tacr1^{+}$ neurons suppresses hyperknesis/alloknesis (control, n = 7; ablated, n = 7) and spontaneous scratching (control, n = 9; ablated, n = 7) in dry skin itch. (G) Silencing $FoxP2^{PBN}$ neurons reduces hyperknesis/alloknesis (eGFP, n = 7; hM4D, n = 7) and spontaneous scratching (eGFP, n = 6; hM4D, n = 7) in allergic contact dermatitis. Error bars represent SEM. Statistical differences were assessed by two-tailed unpaired t-tests (A-G) or two-way ANOVA with Šidák post hoc correction (H). *$p < 0.05$; **$p < 0.01$; ***$p < 0.001$; ****$p < 0.0001$; ns, no significant difference.

Author Manuscript Author Manuscript Author Manuscript Author Manuscript

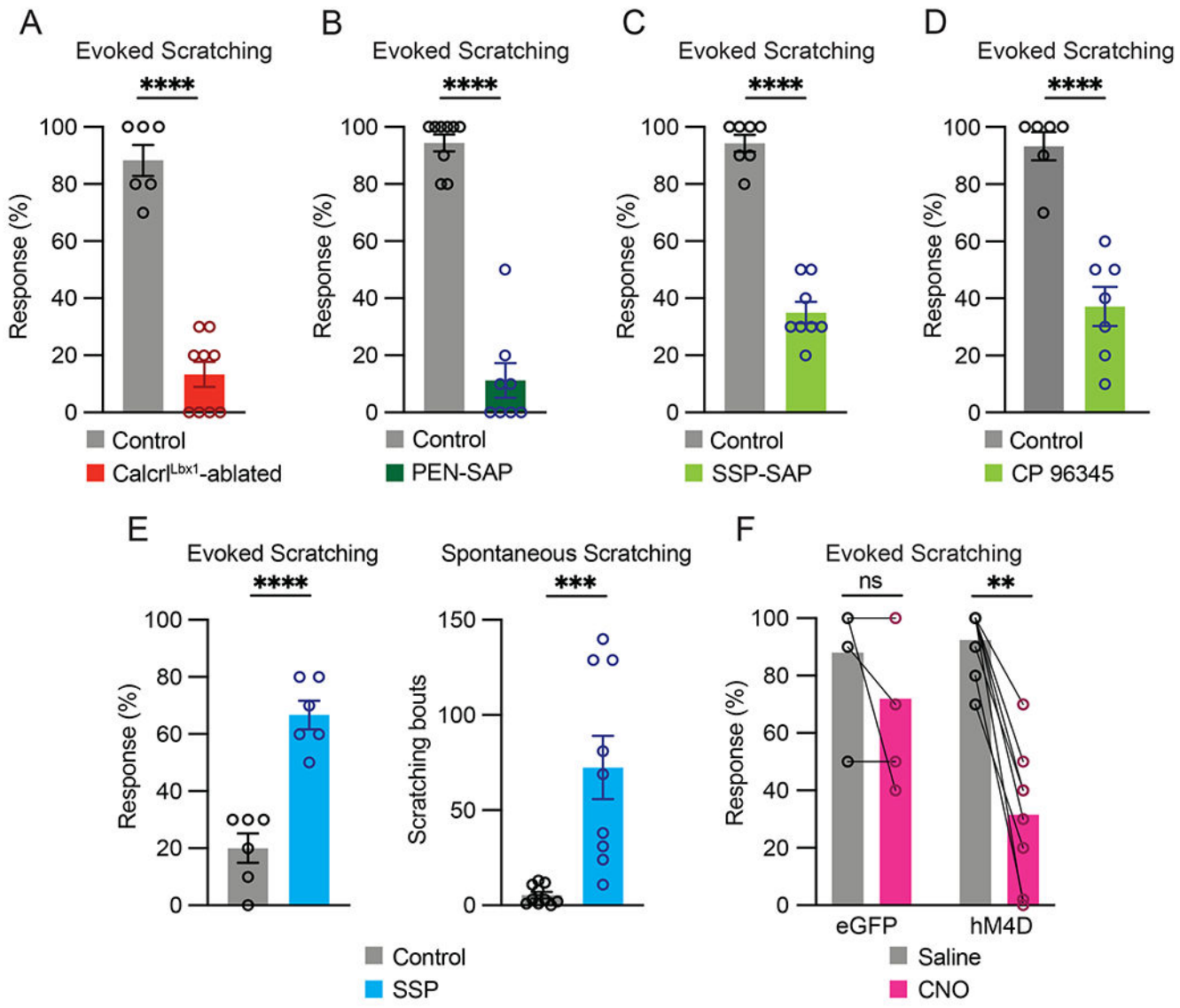

Figure 8. Both the mechanical and chemical itch pathways are required for transmission of acute hyperknesis/alloknesis

(A-D) Acute hyperknesis/alloknesis induced by intradermal histamine is reduced following ablation of Calcrl^{Lbx1} neurons (A; control, n = 6; ablated, n = 9), Gpr83^{+} neurons (B; control, n = 9; ablated, n = 8), and Tacr1^{+} neurons (control, n = 7; ablated, n = 8) and by inhibition of Tacr1 by (control, n = 6; CP 96345, n = 7). (E) Activation of Tacr1 causes hyperknesis/alloknesis (vehicle control, n = 6; SSP, n = 6) and spontaneous scratching (control, n = 10; SSP, n = 9). (F) Silencing FoxP2^{PBN} neurons reduces acute hyperknesis/alloknesis (eGFP, n = 5; hM4D, n = 8). Error bars represent SEM. Statistical differences were assessed by two-tailed unpaired t-tests (A-D) or two-way ANOVA with Šidák post hoc correction (E). **p < 0.01; ***p < 0.001; ****p < 0.0001; ns, no significant difference.

Author Manuscript Author Manuscript Author Manuscript Author Manuscript

KEY RESOURCES TABLE

Antibodies		
Rabbit α-Calcrl (1:50)	Invitrogen	Cat # PA5-52511; RRID: AB_2639234
Mouse α-cFos (1:500)	Abcam	Cat # ab208942; RRID: AB_2747772
Goat α-CTb (1:4000),	List Laboratories	Cat #703; RRID: AB_10013220
Rabbit α-DsRed (1:1000)	Clontech	Cat # 632496; RRID: AB_10013483
Rabbit α-FoxP2 (1:500)	Sigma	Cat # HPA000382; RRID: AB_1078908
Chicken α-GFP (1:000)	Aves	Cat # GFP-1020; RRID: AB_10000240
Rabbit α-Gpr83 (1:500)	Alomone Labs	Cat # AGR-053; RRID: AB_2876803
Chicken α-LacZ (1:1000)	Abcam	Cat # ab9361; RRID: AB_307210
Mouse α-NeuN (1:1000)	Millipore	Cat # MAB377; RRID: AB_2298772
Rabbit α-NK1R (1:500)	Advanced Targeting Systems	Cat # AB-N33ap; RRID: AB_458739
Rabbit α-NPY (1:1000)	Peninsula Lab	Cat # T-4070.0050; RRID: AB_518504
Mouse α-PSD95 (1:500)	Millipore	Cat # MAB1598; RRID: AB_94278
Rat α-RFP (1:1000)	Chromotek	Cat # 5F8; RRID: AB_2336064
Fluorescent *In Situ* Hybridization Reagents		
RNAscope Multiplex Fluorescent Reagent Kit v2 Assay	Advanced Cell Diagnostics	Cat # 323100
EGFP-sense-C2	Advanced Cell Diagnostics	Cat # 409971-C2
Mm-Calcrl	Advanced Cell Diagnostics	Cat # 452281
Mm-Calcrl-C3	Advanced Cell Diagnostics	Cat # 452281-C3
Mm-Gpr83	Advanced Cell Diagnostics	Cat # 317431
Mm-Tacr1-C3	Advanced Cell Diagnostics	Cat # 428781-C3
Virus Strains		
AAVDJ-CMV-eGFP	Salk Institute Viral Vector Core	N/A
AAVDJ-hSyn-HA-hM4D(Gi)-mCherry	Salk Institute Viral Vector Core	N/A
AAVDJ-Syn1-DIO-eGFP	Salk Institute Viral Vector Core	N/A
AAVDJ-EF1a-DIO-hM4D(Gi)-mCherry	Salk Institute Viral Vector Core	N/A
AAV1-hSyn-FLEX-TVA-P2A-eGFP-2A-oG	Salk Institute Viral Vector Core	N/A
EnvA G-deleted Rabies-mCherry	Salk Institute Viral Vector Core	N/A
AAV1-hSyn-FLEX-jGCaMP7s-WPRE	Addgene	Plasmid ID 104491
AAV1-hSyn-DIO-eGFP	Addgene	Plasmid ID 50457
rAAV2-CAG-eGFP	Y Liu	N/A
Chemicals, Peptides, and Recombinant Proteins		
NeuroTrace 435/455	Invitrogen	Cat # SA1011
Cholera Toxin Subunit B (Recombinant), Alexa Fluor 647 Conjugate	Invitrogen	Cat # C34778
Biocytin (ε-Biotinoyl-L-Lysine)	Invitrogen	Cat # B1592
Streptavidin-Cy5	Invitrogen	Cat # SA1011
Diphtheria Toxin, Unnicked, from *Corynebacterium diphtheriae*	List Laboratories	Cat # 150

Author Manuscript Author Manuscript Author Manuscript Author Manuscript

Clozapine *N*-oxide	Sigma	Cat # C0832
Blank saporin	Advanced Targeting Systems	Cat # IT-21
[Sar^9, Met(O$_2$)^{11}]-substance P-saporin	Advanced Targeting Systems	Cat # IT-11
PEN-biotin	CytoLogistics	N/A
Streptavidin-ZAP	Advanced Targeting Systems	Cat # IT-27
PEN (mouse)	Tocris	Cat # 6308
BIBP 3226 trifluoroacetate	Tocris	Cat # 2707
CP 96345	Tocris	Cat # 2893
[Sar^9, Met(O$_2$)^{11}]-substance P	Tocris	Cat # 1178
Tetrodotoxin	Tocris	Cat # 1078
4-aminopyridine	Tocris	Cat # 0940
Chloroquine diphosphate	Sigma	Cat # C6628
Histamine	Sigma	Cat # H7125
Compound 48/40	Sigma	Cat # C2313
SLIGRL-NH$_2$	Abcam	Cat # ab120176
Serotonin hydrochloride	Tocris	Cat # 3547
ß-alanine	Sigma	Cat # 146064
Complete Freund's Adjuvant	Sigma	Cat # F5881
Experimental Models: Organisms/Strains		
Mouse: *Calcrl^{iCre}*	Reference 26	N/A
Mouse: *FoxP2^{Cre}*	Reference 84	JAX stock # 030541; RRID:IMSR_JAX:0 30541
Mouse: *NPY::Cre*	Reference 4	N/A
Mouse: *Lbx1^{FlpO}*	Reference 4	N/A
Cdx2::FlpO	Reference 25	N/A
Mouse: *Ai14$^{lsl\text{-}tdTom}$*	The Jackson Laboratory	JAX stock # 007908; RRID:IMSR_JAX:0 07908
Mouse: *Ai65$^{ds\text{-}tdTom}$*	The Jackson Laboratory	JAX stock # 021875, RRID:IMSR_JAX:0 21875
Mouse: *R26$^{ds\text{-}Syp}$* (*RC::FPSit*)	Reference 87	JAX stock # 030206; RRID:IMSR_JAX:0 30206
Mouse: *R26$^{ds\text{-}hM3D}$*	The Jackson Laboratory	JAX stock # 026942; RRID:IMSR_JAX:0 26942
Mouse: *R26$^{ds\text{-}hM4D}$*	Reference 4	N/A
Mouse: *R26d$^{s\text{-}ReaChR}$*	Reference 89	JAX stock # 024846; RRID:IMSR_JAX:0 24846
Mouse: *Tau$^{ds\text{-}DTR}$*	Reference 25	N/A
Software and Algorithms		
Adobe Illustrator and Photoshop CS5	Adobe	http://www.adobe.com
Prism 5	GraphPad	https://www.graphpad.com
Excel 365	Microsoft	https://www.microsoft.com
ImageJ Cell Counter Plugin	Kurt de Vos, Univ. of Sheffield, UK	https://imagej.nih.gov/ij
pClamp10.4 and Clampfit	Molecular Devices	https://www.moleculardevices.com